Accepted Manuscript

Geo-pedological contribution to the reconstruction of Holocene activity of Chaitén volcano (Patagonia, Chile)

Enrico Casati, Michele D'Amico, Ludek Šefrna, Luca Trombino, Annalisa Tunesi, Franco Previtali

PII: S0895-9811(19)30091-4

DOI: https://doi.org/10.1016/j.jsames.2019.102222

Article Number: 102222

Reference: SAMES 102222

To appear in: *Journal of South American Earth Sciences*

Received Date: 20 February 2019

Revised Date: 29 May 2019

Accepted Date: 29 May 2019

Please cite this article as: Casati, E., D'Amico, M., Šefrna, L., Trombino, L., Tunesi, A., Previtali, F., Geo-pedological contribution to the reconstruction of Holocene activity of Chaitén volcano (Patagonia, Chile), *Journal of South American Earth Sciences* (2019), doi: https://doi.org/10.1016/j.jsames.2019.102222.

Geo-pedological contribution to the reconstruction of Holocene activity of Chaitén Volcano (Patagonia, Chile)

Enrico Casati[1*]; Michele D'Amico[2]; Ludek Šefrna[3]; Luca Trombino[4]; Annalisa Tunesi[1]; Franco Previtali[1]

[1] Department of Earth and Environmental Sciences, University of Milano - Bicocca, Italy
[2] DISAFA, University of Torino, Italy
[3] Department of Physical Geography and Geoecology, Charles University, Prague, Czech Republic
[4] Department of Earth Sciences, University of Milano, Italy

[*] Corresponding author: enrico.casati@unimib.it

Keywords: Paleosols, Geochemistry, Tephra, Chaitén Volcano, Michinmahuida Volcano.

Abstract

On May 2, 2008, the Chaitén volcano, located in Chilean Patagonia, thought to be inactive for almost 10,000 years, erupted, emitting pyroclastic materials (ash and pumice) of rhyolitic composition. The ejected materials partially burned the forest vegetation in a wide radius, blocked the river systems, causing local flooding, and forced the majority of the inhabitants to abandon the nearby village of Chaitén.

In 2005 and 2009, the authors surveyed and sampled a number of paleosols and tephra sections located just north of the village. The present work shows the results of pedological, micromorphological, petrographic, and geochemical analyses, accompanied by radiocarbon dating, The studies have shown the presence of different soil complexes (Andosols), developed from pyroclastic materials and separated by erosional surfaces. Under the modern soil, consisting only of A horizons, paleosols follow with pedogenized horizons overlying altered and hardened volcanic materials. The mineralogical and geochemical analyses confirmed the sequence of these complexes and distinguished a double origin of the materials from which they developed: the most recent and superficial soil, although not significantly affected by the depositions of the last eruption, presented an evident geochemical and mineralogical affinity with tephra of the Chaitén volcano, differently from those of the deeper paleosols which have been found to derive from the ejecta of Michinmahuida volcano. The evolutionary model of the soils of the area has also been confirmed by the dates measured along the studied sections that are comparable with the dates of volcanic events during the Holocene already ascertained by the most recent volcanological studies..

1. Introduction

The area under investigation is dominated by the presence of two main volcanoes, Michinmahuida and Chaitén that are located respectively about 25 km to the north-northeast and 11 km to the northeast of the Chaitén village in Chilean Patagonia (Fig. 1). Michinmahuida is a massive ice-covered stratovolcano whose products are mainly from intermediate to basic composition. Chaitén is a small volcano which, before 2008, was characterized by a rhyolitic (obsidian) lava dome preserved within a 3 km in diameter central caldera. Minimum emplacement age of the lava dome (older than 5.6 kyr) was inferred by obsidian archeological artifacts, attributed by Stern et al. (2009) and Stern (2008) to the Chaitén dome and found in the Chan Chan site (400 km north of Chaitén) occupied from 5.6 to 5.0 kyr. On May 2, 2008, the Chaitén volcano violently erupted after less than 36 h of precursory seismicity (Lara, 2009; Tilling, 2009; Pallister et al., 2010; Romero, 2011). The ash plume, directed to the SE, was about 15 km high and the ash-fall covered a wide region around the volcano, reaching Argentina up to its Atlantic coasts (Watt et al., 2009; Lara, 2009; Carn et al., 2009; Martin et al., 2009). The explosive activity lasted the whole month and tephra falls, floods and lahars caused extensive damage to the river network and forest cover and forced the majority of the local residents to leave the Chaitén village. Because the volcano was considered quiescent for almost 10,000 years (Naranjo and Stern, 2004), the 2008 explosive activity was unexpected and led the scientific community to search for evidence of other eruptions during the Holocene.

After new surveys in the concerned region (Watt et al., 2011; Amigo et al., 2013; Lara et al., 2013; Watt et al., 2013; Major and Lara, 2013; Moreno et al., 2015, Alloway et al., 2017a, 2017b) new hypotheses on Chaitén volcanic activity have been proposed: rhyolitic tephra deposits were identified and radiocarbon age determinations suggested a frequent eruptive activity throughout the Holocene up to the 17th century.

The present contribution analyzed 3 soil profiles, located near the Chaitén village, sampled before 2008 Chaitén eruption and reviewed on 2009. The profiles were studied through pedological investigations and the results were compared with those inferred from mineralogical and geochemical data (mainly REE concentrations and trace elements ratios) to define the provenance of volcanic materials found in soil horizons.

2. Materials and methods

2.1 *Study area description*

The area under investigation (Fig. 1) belongs to the Southern Volcanic Zone (SVZ) of the Andes, between latitudes 33° and 46°S, and is the result of the subduction of the Nazca plate beneath the South America continental plate. The subduction-related magmatism has been active since mid-Jurassic times and is represented by the Early Cretaceous – late Cenozoic Northern Patagonian Batholith (Pankhurst et al., 1999; Hervé et al., 2007) that intruded late Paleozoic to Early Mesozoic metamorphic rocks (Adriasola et al., 2005), the Jurassic-Eocene arc and back-arc volcanism (Parada et al., 2001) and the Holocene volcanism. In the SVZ region, thirteen volcanoes are associated with Pleistocene-to-recent magmatism. Most of the volcanic centers (Cay, Mentolat, Melimoyu, Yate, Huequi, Michinmahuida, Hudson) erupted high-Al basalts with subordinate andesites and dacites (Naranjo and Stern, 1998; D'Orazio et al., 2003; Stern, 2008); rhyolites are rare and associated with Chaitén (Kilian and López-Escobar, 1991; Castro and Dingwell, 2009; Watt et al., 2009; Alfano et al., 2011), Yate (Mella Barra, 2008; Watt et al., 2011), Puyehue-Cordón Caulle (Lara et al., 2006; Singer et al., 2008; Castro et al., 2013) volcanic activity. The roughly N-S distribution of these centers suggests that their emplacement may be related to the Liquiñe-Ofqui fault zone (Thiele et al., 1986; López-Escobar and Moreno, 1994; Wicks et al., 2011), a 1000 km NNE-SSW dextral strike-slip fault system joined by a series of *en-échelon* lineaments striking NE-SW (Cembrano et al., 1996).

The surveyed area is located on a gently undulating surface west of the Chaitén riverbed. The whole area is drained by three rivers - Rio Chaitén, Rio Negro and Rio Yelcho - flowing into the gulf of Chaitén and forming a digitated delta-estuary. Cool summers and a lack of dry seasons characterize the oceanic temperate climate (*Cfb*-type) of Andean Patagonia (Peel et al., 2007). In northern Patagonia (40°– 48°S latitude) rainfalls are mainly due to strong moisture-laden air flows from the southern Pacific Ocean and increase with altitude (Garreaud, 2009).

In the investigated area, long-term precipitation data are lacking. Pierson et al. (2013) report a range from 2500 to 7000 mm/yr during 2005-2009. The frequent volcanic activity in the Southern Andes influences the local weather, especially the occurrence of heavy rainfalls. During the last explosive phase of the Chaitén volcano (May 2008) rainfall delivered 600–900 mm of precipitation over 12 days, with a daily maximum of about 120 mm (Pierson et al., 2013). The monthly average temperature in Puerto Montt (about 160 km north-northwest of Chaitén) is 20°C during the hottest months (January and February) and 3°C in the coldest month (July), with an annual average temperature between 8.5 and 9°C (Dirección Meteorológica de Chile, 2001*).*

2.2 Soil and paleosols sampling and analyses

Three soil/tephra/paleosols sections (P16, P17 and P18) were studied and analyzed, in an area close to Chaitén village (Fig.1; Tab.1).

Field investigations and descriptions (FAO, 2006; Schoeneberger et al., 2012) allowed recognizing several horizons characterized by different degrees of pedogenesis and weathering of pyroclastic parental materials. Soil horizons and tephra layers were named according to the World Reference Base for Soil Resources (IUSS Working Group WRB, 2015).

Twenty-four samples were collected from pedogenic horizons and tephra layers in all the described sections.

Chemical, mineralogical and geochemical analyses were performed on selected samples. Other volcanic and rocky materials were sampled and analyzed for geochemical comparison in order to ascertain the provenance of the materials: three samples from 2008 Chaitén eruption (CHA-1, CHA-2, CHA-3); one sample from Laguna Pinto Concha area, close to Hornopirén village (LP-1); two samples collected along the Rio Amarillo which drains the slopes of Michinmahuida volcano (MIC-1, MIC-2); one sample from the Corcovado volcano (COR-1); one sample of granodiorite, bedrock of P18 profile (R-GRD) (Tab. 1). Soil chemical data were obtained according to standard methods (van Reeuwijk, 2002).

Four undisturbed samples from deep horizons in profile P16 (2Bt, 3CBd) and P17 (2Btgd, 3CBd) were impregnated (according to Murphy, 1986) for thin section morphological analyses (Bullock et al., 1985; Stoops, 2003).

Two samples of P18 profile (AE, 5CBd) were investigated through X-ray diffraction. Spectra were obtained on total soil powder and on fractions below 60 µm and between 60 and 250 µm. Random oriented powders were analyzed with a Panalytical XPERT-PRO PW 3050 X-ray diffractometer with Cu Kα radiation at 40 kV and 40 mA (a counting time of 71 s per 0.02° step was used for 2θ in the 4–70° range). Two polished thin sections were prepared on fraction above 250 µm and representative minerals, lithics and glass were analyzed for major and minor elements using a JEOL 8200 Superprobe at University of Milano. Analytical conditions were optimized for standard silicates and oxides on wavelength-dispersive spectra at 15 kV and 5 nA.

Horizons and layers recognized in the field were analyzed for major, minor and trace elements at ACME Laboratories in Canada. Analytical methods are described at www.acmelab.com. For geochemical considerations, all major elements of P16, P17 and P18 samples were recalculated on volatile free basis. Primitive Mantle (PM) and Chondritic (Ch) values for Rare Earth Elements (REE) are from Sun and McDonough (1989).

The chemical index of alteration (CIA) (Nesbitt and Young, 1984) was calculated according to the formula:

$$CIA = [Al_2O_3 / (Al_2O_3 + CaO^* + Na_2O + K_2O)] \times 100$$

where oxides are expressed as molar proportion and CaO* is the content in silicate minerals only. The CIA index represents the degree of alteration of feldspars to clay minerals in the course of hydrolytic weathering, and indicates the relative contents of clay minerals. Values for unweathered igneous rocks are about 50, whereas intensely weathered materials rich in kaolinite and gibbsite can approach 100.

From the total geochemical compositional data, rare earth elements content and distribution have been observed to detect lithological discontinuities and different tephra origins.

A cluster analysis (average linkage method, Euclidean distance) was performed based on geochemical composition data, in order to detect similarities in geochemistry between soil horizons and tephra origins. The vegan package (Oksanen et al., 2017) in the R software was used.

Five radiocarbon ages were obtained from organic matter fractions (humins and humic acids) extracted from P16, P17, P18 selected horizons at the Poznan Radiocarbon Laboratory (www.radiocarbon.pl), with the AMS technique for sample preparation. All data were given as calibrated years BP using OxCal4.2 (Bronk Ramsey and Lee, 2013) and the Southern Hemisphere calibration curve SHCal04 (McCormac et al., 2004). BP refers to years before 1950 A.D. Results are quoted at 95.4% confidence intervals.

3. Results

3.1. Landforms and features of soil profiles

Pedological and physical features of the studied sections are summarized in Tab. 2.

The sequence of the P16 consisted of six complexes composed of tephra layers and buried pedogenic horizons (Fig. 2, Fig. 3a; Tab. 2). From the surface to the depth of 30 cm the horizons Oi and Ah are typical of modern volcanic soils. From 30 to 125 cm a weathered horizon 2Bwh and an illuvial 2Bt occurred, both belonging to an independently evolved soil profile developed from tephra and truncated at the top by ancient erosion processes. From 125 cm to 245 cm, a pedogenized and hardened cineritic layer, 3CBd, was recognized. A layer of moderately weathered lapilli (4C) occurred at a depth between 245 and 265 cm, underlain by a thin layer (5Csm), extending from 265 to 270 cm, of partially cemented and weathered ferruginous ash. Between 270 and 275 cm, grey weathered ashes (6C) lied on grey unweathered metapelites. All layers and buried soil horizons had a field assessed sandy texture. Measured pH(H_2O) values ranged from 4.2 (extremely acidic) on the surface to 5.7 (moderately acidic) at depth, associated with the very low base saturation value (3-9%) due to heavy leaching caused by local strong rainfall. The pH(NaF) exceeded the critical value of 9.5 (Tab. 3) along the entire profile indicating abundance of allophane and/or Al-organic complexes in mineral horizons (IUSS Working Group WRB, 2014).

Eight complexes were recognized in the P18 profile (Fig. 2, Fig. 3b; Tab. 2). From the surface to the depth of 30 cm the horizons (Oi-Ah-AE) were rich in organic matter and showed features of modern pedogenesis. Only P18 AE horizon was strongly depleted in Al (both total and oxalate extractable), and showed a low pH(NaF), evidencing possible leaching associated with incipient podzolization.

From 30 to 180 cm, after a sharp erosional limit, three buried organic matter-rich B horizons (2Bwh1-2Bwh2-2Bth), developed from older tephra deposits. A thin horizon (3Oa) of highly decomposed organic material and an equally thin ferruginous cemented ashy horizon (4Bsm) separated at 185 cm the older section, mainly represented by weakly pedogenized to hardened cineritic horizons extending as far 290 cm. Three C horizons occurred, composed of weakly weathered tephra materials, with different degrees of cementation. The 8C horizon (325-345 cm) was mainly composed of ash with volcanic lithics and few granodiorite fragments. It represents the basis of the P18 sequence and is lying on the sheep-back shaped and unweathered granodiorite (R-GDR).

Although P18 had more organic matter through the upper 2 meters, chemical characters were almost similar to P16, confirming strong leaching and high content in allophane or Al-organic complexes.

P17 profile (Fig. 3c) showed similar features and stratigraphy but the weathered old soil was thicker (3 meters) than in P16 and P18 and no substrate was exposed. Under a 35 cm thick surface Ah horizon, six B horizons developed down to 340 cm including (top to the bottom) weathered (2Bwh sequence), illuvial (2Bth sequence) and gleyed, hardened (2Btgd) horizons. Underneath up to 380 cm very hard ashy materials (4CBd) occurred.

The correlation between three schematic groups of horizons among the three described sections are shown in Fig.2: modern volcanic soils on the top (group I); weathered, well developed older soils (group II); weakly pedogenized, cemented tephra and bedrock (group III).

3.2. Micromorphology

The abundance of volcanic fragments in the coarse fractions and the undifferentiated b-fabric of the micromass confirm the volcanic origin of the parent materials of the P16 and P17 profiles (Sedov et al., 2010). All thin sections showed isotropic clay coatings and infillings. Their presence was related to pedogenic processes (i.e. amorphous clay illuviation) or in situ precipitation of Al and Si (i.e. authigenic clay coatings, Sedov et al., 2010). Redoximorphic features (small Fe-Mn nodules and few Fe-Mn hypocoatings and impregnations) were also observed in all samples.

P16-2Bt and P17-2Btg showed a fair degree of past pedogenic development and it was characterized by angular blocky structure and microstructure, biogenic channels, some rounded phytorelicts and isotropic clay coatings and few pore infillings. The coatings were also visible at the macroscopic scale. These features appeared to be indicative of long-term clay illuviation. A few reddish or dark Fe-Mn nodules and impregnations were also observed. Some pore walls had layered spongy reddish coatings, probably composed of amorphous materials likely associated with organic matter (Fig.4a).

On the contrary, the P16 3CBd and P173BCd horizons had a sandy-silty appearance and was mainly composed of volcanic materials with few clay coatings (illuvial or authigenic in origin), thus suggesting a weak pedogenic development. No aggregation was observed at the microscopic scale. A few opaline bodies were observed within the hard groundmass (Fig.4b).

3.3. Mineralogy

The mineralogy of P18-AE and P18-5CBd horizons was determined by X-ray diffraction, thin sections and mineral chemistry (Tabs. S1 to S5). Mineral abbreviations are after Whitney and Evans (2010).

XRD patterns (Fig. 5a) of P18-AE showed significant amount of glass and negligible quantities of clay minerals. Prevalent phases were: glass, quartz (Qz), cristobalite (Crs), plagioclase (Pl) and augite (Aug). Crs was mainly concentrated in the fraction below 60 μm; on the contrary, Qz prevailed in the fraction between 60 and 250 μm. The thin section analysis of the fraction above 250 μm revealed glass, crystals and lithics which did not show evidence of weathering. Olivine was absent. Fragments of crystals (0.6-0.8 mm in size) were mainly constituted by green clinopyroxenes (Cpx, Fig. 6a) and colorless orthopyroxenes (Opx). Both pyroxenes showed large compositional variation: mg-number for Opx ranged from 58 to 73 and Cpx from 63 to 77. Opx with enstatite (En) content lower than 60% was detected in thin crystals within glass shards. Pl was slightly zoned (cores An 43-44% and rims An 38-41%) and locally showed resorbed structures. Rare crystals of deep-brown hornblende occurred (Fig. 6a). These amphiboles were not euhedral and lacked marginal reaction rims. They were ferri-titanian-tschermakite, were Al-rich (11.56-11.78 wt%) and had TiO_2 up to 3.26 (wt%). Angular lithics were represented by deformed polycrystalline aggregates and granodiorite fragments (Fig. 6b) similar to the bed-rock of P18 site. Qz, green Hbl, Pl with deformation twinnings (oligoclase An 30-32%), biotite (Bt), K-feldspar (Kfs) and Qz are the main phases in granodiorite fragments. Most of the lithics (0.5-1.0 mm in size) were well rounded and oxidized volcanic rocks. In a lesser amount, fragments were constituted by well-preserved volcanics with thin laths of Pl (An 34-37%). Glass shards were highly vesicular (Fig. 6c) and showed strong fluidal textures. In these fragments, small microphenocrystals of Pl (An 43-50%) were recognized. The glass was rhyolitic in composition but had lower silica content with respect to pumice and glassy block fragments of 2008 eruption (70% and > 75% respectively). All analyzed glasses were slightly peraluminous (with normative corundum).

Diffractogram (Fig. 5b) of P18-5CBd showed clay minerals mainly in the fraction between 60 to 250 µm characterized by a peak for possible interlayered vermiculite- or smectite-illite minerals at around 6°2 θ (ca. 24 Å). Main phases were plagioclase (Pl) and augite (Aug). Thin section (above 250 µm fraction) showed that tephras were more oxidized, generally covered with patina and had finer grain size (between 0.4 and 0.6 mm) than those identified in sample P18-AE. Weathered rounded fragments of volcanic rocks prevailed on crystals. The volcanic lithics had Pl (An 61-68%), Cpx and Ol (±Opx). Opx showed limited variation and the mg-number falls within a very narrow range (72-73) indicating no significant zoning; on the contrary Cpx has a wider mg-number range, between 64 and 75, CaO content decreases with FeO increasing. Colorless glass shards are mainly dacitic in composition and present Fe-enrichment. The brown glasses have thin laths of Pl (An 50-54%) and Ol (Fo 69%), present low silica content (basaltic-andesite), are metaluminous and are enriched in TiO_2, MgO, FeO, CaO. Pl, Ol and Cpx mainly constitute crystal fragments. No granodiorite lithics were found. In this sample, olivine presents two different compositions (Fig. 6d). Pale-green, generally isolated (single) crystals with dark-brown glass inclusions (rhyolitic in composition) reveal low forsterite (Fo) content ranging from $Fo_{19.8}$ and $Fo_{22.6}$. The low Fo content is coupled with high MnO content (2.4-2.6 wt%). No NiO was detected. Colorless olivines are instead present as phenocrystals in volcanic lithics (Pl, Px, Ol and basaltic-andesite glass). These olivines have Fo which spans from $Fo_{68.7}$ to $Fo_{70.3}$ and present low contents of MnO and NiO (0.40-0.51 wt%, < 0.14 wt% respectively).

3.4 Geochemistry

Elemental analysis (Tab. 4) of the three soil/paleosols profiles and of other rock samples from different volcanoes in the area clearly showed the difference between soil horizons and lithic materials. The first were characterized by large loss on ignition (LOI), and high contents of C, derived from organic materials since all samples are carbonate-free; Ca content was derived only from silicate minerals.

The three groups identified through pedological approaches are also supported by geochemical data.

The topsoil horizons (group I, P18: Ah, AE; P16-Ah) had low CIA values, ranging from 51 and 61. The intermediate horizons (group II, P16: 2Bwh, 2Bt; P18: 2Bwh1, 2Bwh2, 2Bth, 3Oa) form a separate cluster and showed an advanced degree of weathering with CIA between 81 and 86 units. The upper two horizons of group III (P16: 3CBd, 4Cr, 5Csm; P18: 4Csm, 5CBd, 6Cr, 7Cs, 8C) had low CIA values (59 and 55) in P18 profile, but were higher in P16 profile (70-61). The lowermost layers P16-5Csm and P18-7Cs presented CIA values (70) approaching those calculated for group II samples.

Other geochemical tools, such as concentration of major and trace elements, rare earth elements (REE), rock-chondrite ratios confirm the existence of distinct groups and different volcanic sources of parental material.

On volatile free basis the silica content of group I samples was about 70 wt% with low MgO and TiO_2 contents. Major elements suggest a slightly peraluminous rhyolitic composition of the parental material. These samples were characterized by large-ion lithophile elements (LILE) enrichments and low contents in compatible elements such as Cr, Ni, Sc and V. The REE contents (Fig. 7a) were generally low (ΣREE 76-81 ppm) with enrichment in light rare earth elements (LREE) (66-69 ppm) over heavy rare earth elements (HREE) (5-6 ppm), $(La/Yb)_N$ between 8.07 and 10.54 and negligible Eu anomaly (Eu/Eu* = 0.74-0.86). On a PM-normalized spider diagram (Fig. 7b), all samples show similar patterns with well-developed K and Pb positive peaks, troughs at Nb-Ta, Ba, and P and peaks at Th-U and Nd-Zr.

The group II horizons had the highest Al_2O_3 but the lowest SiO_2 and alkalis concentrations. In P18 profile, Al_2O_3 contents increased and Fe_2O_{3tot} decreased downward whereas both these oxides were quite constant in P16 profile (~32 and 18 wt % respectively). On volatile free basis, all these samples revealed low silica contents consistent with basic composition. All samples, with respect to group I horizons, showed LILE depletion, particularly in Rb and Ba, and higher values of Cr, Ni, Sc and V (up to 55, 22, 41, 346 ppm respectively). The REE contents (Fig. 7c) were from 105 and 144 ppm. LREE (78-111 ppm) were higher than HREE (14-20 ppm), but the patterns were smooth with $(La/Yb)_N$ ratios varying from 1.71 and 4.23. Eu/Eu* ranged between 0.84 and 0.86. On a PM-normalized spider diagram (Fig. 7d), all these samples showed similar patterns with well pronounced troughs at Rb-Ba, Sr-P. The Nb-Ta was less marked because of negative K anomaly. Pb positive peak was similar to those shown by group I horizons.

The group III deepest horizons (on volatile free basis) were characterized by silica ranging from 44 up to 54 wt% suggesting a basaltic or basaltic-andesite composition and presented high MnO (0.2-0.3 wt%) and P_2O_5 (up to 0.72 wt%) contents. Compared with group II samples, group III shows a more pronounced LILE enrichment (Fig. 7f). Lowest horizons of both profiles (P18-6C and P16-5Csm) had the highest Nb contents (16-19.3 ppm), Zr (306-405 ppm), Y (53.8-65.9 ppm), Hf (8.6-10.9 ppm). The ΣREE ranged from 147 and 279 ppm. A LREE (117-226 ppm) enrichment and a relative depletion in HREE (13-29 ppm) were observed. Samples show a more fractionated trends with $(La/Yb)_N$ ratios varying between 3.32 and 4.68 (sample P18-8C= 6.36) and a more pronounced Eu anomaly (Eu/Eu* = 0.68-0.86, Fig. 7e) with respect to group II. The P18-8C presented silica content of about 60 wt%, lower Al_2O_3, P_2O_5, and MnO contents than other levels of group III. This could be explained by the large amount of granodiorite lithics that masks the real composition of tephra.

3.5 Dating

Radiocarbon datings were measured at different soil depths in P16, P17 and P18 respecting the horizon sequence as defined in the three described main groups (Tab. 5).

The youngest ages were obtained from the surface rhyolitic-dacitic horizons (P18-Ah and P18-AE), dating 345±30 ^{14}C yr BP and 1320±30 ^{14}C yr BP respectively. Calibrated ages range from 454-304 yr BP to 1283-1087 yr BP, corresponding to 1571±75 AD for the surface horizon and 765±98 AD for the lowermost.

The P17-3CBd horizon, although sampled at the greatest depth (-340cm) represents the upper level of the third group of horizons and gave an age of 7670±60 ^{14}C yr BP, with a calibrated age ranging between 8558 and 8317 yr BP (8.6-8.3 kyr BP). The Fe-cemented P16-5Csm (-270 cm) yielded a radiocarbon age of 8230±60 ^{14}C yr BP and a calibrated age between 9397 and 8998 yr BP (9.4-9.0 kyr BP). The last one is comparable with the P18-7Cs horizon (-306 cm), that gave an age of 9110±60 ^{14}C yr BP and a calibrated age between 10407 and 9935 yr BP (10.4-10.0 kyr BP).

4. Discussion

All the analyses converge to the identification of two main sources of volcanic materials composing the studied soil-tephra sections. Field and pedological evidences (chemical analysis and micromorphologic interpretations) describe the alternation of polycyclic soil-forming events and erosional phases. Beneath modern A horizons, B horizons were characterized by a stronger weathering of volcanic products, by clay formation and its downward translocation. In depth weakly weathered CB horizons stood over C layers of lapilli and ashy materials in evident discontinuity with the bed-rock, only partially involved in soil genesis. Although P16 and P18 profiles did not have the same horizon sequence, they a showed similar pedogenic history. In these profiles, Ah horizons were characterized by high pH(NaF), high value of Feo/Fed ratio and low value of the (Fed-Feo)/Fetot. These indexes and the low base saturation suggest a low degree of pedogenic development, corresponding to the characters of Dystric Vitric Andosols. Moreover, Al and Fe leaching characterizes P18-AE horizon, and considering the low pH(NaF) should be associated with an incipient podzolization (Zúñiga et al., 2019). A and B horizons were separated by a sharp erosional surface. B horizons are illuvial and can be interpreted as a preserved part of former Dystric Silandic Andosols developing towards Alisols (Andic). The surface horizons of the P17 section presented andic properties with a high pH(NaF) value, that characterizes a Dystric Silandic Andosol, while the underneath sequence of B horizons fits well with the preserved part of a Dystric

Bathigleyic Silandic Andosol developing towards Alisols (Andic). The deepest layers in all the three sections were represented by hardened CBd horizons, relict hardpans (locally known as tepetate or cangahua) preserved after another erosional event. This local pedomarker was separated from the above standing horizons by a sharp erosional surface: few phytorelicts found in the upper part of any of these horizons confirmed the presence of previous eroded horizons.

All the investigated sections show that soils had been influenced by similar pedogenic processes: a strong climatic leaching associated with a low base saturation value and acidic reaction; a high content of paracrystalline minerals, as represented by various Fe ratios and pH(NaF); clay translocation during past periods; cementation of volcanic materials at depth.

According to the processes characterizing all sections, three groups of horizons and layers have been distinguished. In particular, group I includes recent A soil horizons characterized by organic matter association with Al-rich amorphous materials and low CIA values; group II represents quite strongly weathered and/or clay illuviated B horizons with high CIA values; group III gathers hardened weakly pedogenized materials (CB horizons and C layers) with low CIA values.

Mineralogical and geochemical investigations confirm the identification of these three main groups of horizons and allow recognizing two main provenances of volcanic materials. Whole rock data indicate a good correlation among the profiles and cluster analysis (Fig. 8) shows that surface A horizons seem to be associated with Chaitén tephra; another cluster, including most of the deeper horizons, is correlated with dacite from Michinmahuida volcano.

All samples are sub-alkaline with calc-alkaline affinity. PM-normalized multi-element spider diagrams (Fig. 7) show that all samples have LILE enrichment and Nb-Ta anomaly typical of subduction related rocks.

The surface A horizons showed marked differences in petrographic and geochemical characteristics with respect to the lower layers. These horizons have rhyolitic-dacitic composition, are slightly peraluminous, present high La/Yb (11.25-14.70), Rb/Ba (0.16), Ba/Sr (2.86-3.13), Sr/Y (9.9-13.28), Hf/Nb (0.36-

0.40). In the investigated area, three main occurrences of rhyolites are described associated with Chaitén, Yate and Cordón Caulle eruptions. All the geochemical data point to a Chaitén provenance of volcanic materials found in top soil horizons because Yate (this study and Mella Barra, 2008; Watt et al., 2011) and Cordón Caulle (Castro et al., 2013) rhyolites are enriched in ΣREE (Yate >120 ppm, Cordón Caulle > 160, Chaitén <104 ppm), have more pronounced Eu anomaly and higher ratios between refractory elements such as Zr/Nb (Yate 30-34, Cordón Caulle 39-54, Chaitén 12-13) and Nb/Hf (Yate 0.9-1, Cordón Caulle 0.9-3.0, Chaitén 0.3-0.4; Fig. 9). XRD and mineral chemistry also confirms the Chaitén provenance of these materials. Ti-rich brown amphibole and cristobalite were recognized in sample P18-AE. These two minerals were identified in pyroclastic fall deposits following the 2008 Chaitén eruption. In particular, the brown amphibole (high in Al_2O_3 and TiO_2) presents the same features as those described by Lowenstern et al. (2008; 2012). As reported by Reich et al. (2009), Horwell et al. (2010) and Alfano et al. (2011) the 2008 Chaitén ash contains a significant amount of cristobalite as well as P18-AE sample, in which this mineral has been identified through XRD in the fraction below 60 µm (Qz prevails in the coarser fraction)..

With respect to A levels, the group II and group III horizons are more mafic in composition (basalt, basaltic-andesite), present lower LILE but higher HREE contents (14-29 ppm) and are less fractionated (La/Yb_N 1.7-4.5). All these data, element ratios (Fig. 9) and comparison with other volcanos of SVZ of similar composition, suggest that the Michinmahuida is the most probable source of volcanic materials found in B and C horizons. Mineral chemistry data for Michinmahuida products are rare, but Cpx (mg-number 75-64), Ol (Fo_{68-70}) and Pl (An_{68-61}) have composition comparable with those reported by López-Escobar et al. (1993). Furthermore, it is important to point out the occurrence of olivine rich in fayalite (Fo_{22-20}). In the B horizons of the studied sections, this olivine is commonly present as single crystal but, as shown in Fig. 6d, also occurs in lithic fragment associated with plagioclase An_{33}. Two main occurrences of fayalite in evolved rocks of SVZ are reported: Triassic fayalite granites (Vásquez and

Franz, 2008; Vásquez et al., 2009) in the Cobquecura pluton (36°S) and Holocene fayalite rhyolites associated with Cordón Caulle volcano domes (40°32'S, Singer et al., 2008). These rocks are enriched in FeO* over MgO (FeO*/(FeO*+MgO) = 0.91-0.93) as the rhyolitic brown glass inclusions (0.96) found in fayalite-rich olivine. Lower MgO content in glass is coupled with higher Fo content (Fa_{77-80}) in olivine with respect to granites (Fa_{89-98}). On the basis of the available data, the fayalite lithics found in P18-CBd, similar to the fayalite granites of the Cobquecura pluton, could represent basement fragments incorporated into the magma during Michinmahuida eruption.

^{14}C age determinations on P18-Ah1 and P18-AE horizons suggest that the explosive activity of the Chaitén volcano is characterized by two distinct periods of activity: 345±30 yr BP (454-304 calibrated years BP) and 1320±30 ^{14}C yr BP (1283-1087 calibrated years BP) respectively. The first age matches well with the recent radiometric data of Lara et al. (2013), who correlate it with an historical 17th-century (AD 1625-1658) eruption of the Chaitén volcano, and with the data published by Moreno et al. (2015). The event recorded in the P18-AE horizon at 1320±30 ^{14}C yr BP (1283-1087 calibrated years BP) is not been previously documented in any recent research.

Lowermost horizons evidenced three main eruptive events occurred at 10.5-9.9 ka BP, 9.4-9.0 ka BP and 8.6-8.3 ka BP. The oldest age could be related to the “Amarillo ignimbrite” (10.5-10.2 ka BP) event as defined by Amigo et al. (2013), although, in this case, the volcanic material emplaced as tephra fall. The youngest ages are not reported in any recent research, but confirm the continuous eruptive activities of the Michinmahuida volcano.

5. Conclusions

The present paper describes a multidisciplinary approach to the study of the soil evolution in the area just to the north of Chaitén village, in Chilean Patagonia. Chemical, micromorphological, mineralogical, and geochemical analyses led to recognize two different origins of the pedogenized materials, producted by the two main active volcanoes in that area: Chaitén and Michinmahuida.

- The investigated sections present a comparable organization of different soil complexes: modern soil represented by uppermost A horizons, covering an older truncated sequence of weathered and illuvial B horizons, lying in stratigraphic discontinuity on a dense pedomarker horizon formed of weakly weathered tephra. Granodiorite or metapelites form the bed-rock of the sequences.
- All the soils sequences were separated by erosional events.
- Mineral chemistry and geochemical investigations performed on selected samples demonstrate two different provenances of volcanic soil parent materials: the uppermost modern soil complex resembles Chaitén tephra; differently the lowermost older relict soils correlate with the Michinmahuida ejecta.

This model of the soils evolution fits well other recent studies on the volcanic history of the area: ^{14}C dating of our recognized soil complexes results comparable with the age of known volcanic events reported by other cited Authors and confirms the repeated explosive activity of both volcanoes during the Holocene.

Acknowledgements - We sincerely thank: V. Maggi and R. Comolli (Dept. Earth and Environmental Sciences, University of Milano - Bicocca, Italy) for the useful discussions on soil genesis and Holocene climate of Patagonia; F. Moia (Dept. Earth and Environmental Sciences, University of Milano - Bicocca, Italy) for some chemical analyses performed on the tephra samples; Z. Engel (Dept. Physical Geography and Geoecology, Charles University, Prague, Czech Republic) for his geomorphological contributions during the field survey; R. Pini and F. Badino (CNR-IDPA, Milano, Italy) for radiocarbon dating comments and botanical consultancy; S. Andò (Dept. Earth and Environmental Sciences, University of Milano - Bicocca, Italy) for contribution to mineralogical investigations; N. La

Penna (Free-lance, Chaitén, Chile) for his important logistic support given on the field; Dr. L.E Lara and the other unknown Referees for their relevant suggestions.

References

Adriasola, A.C., Thomson, S.N., Brix, M.R., Hervé, F., Stöckhert, B., 2005. Postmagmatic cooling and late Cenozoic denudation of the North Patagonian Batholith in the Los Lagos region of Chile, 41°- 42°15' S. Int. J. Earth Sci. 95, 504-528, doi: 10.1007/s00531-005-0027-9.

Alfano, F., Bonadonna, C., Volentik, A.C.M., Connor, C.B., Watt, S.F.L., Pyle, D.M., Connor, L.J., 2011. Tephra stratigraphy and eruptive volume of the May, 2008, Chaitén eruption, Chile. Bull. Volcanol. 73, 613-630. doi: 10.1007/s00445-010-0428-x.

Alloway, B.V., Moreno, P.I., Pearce, N.J.G., De Pol-Holz, R. Henriquez, W.I., Pesce, O.H., Sagredo, E., Villarosa, G., Outes, V., 2017a. Stratigraphy, age and correlation of Lepué Tephra: a widespread c. 11 000 cal a BP marker horizon sourced from the Chaitén Sector of southern Chile. J. Quat. Scie., 1-35. https://doi.org/10.1002/jqs.2976

Alloway, B.V., Pearce, N.J.G., Moreno, P.I., Villarosa, G., Jara, I., De Pol-Holz, R., Outes, V., 2017b. An 18,000 year-long eruptive record from Volcan Chaitén, northwestern Patagonia: paleoenvironmental and hazard-assessment implications. Quat.Scie.Rev., 168, 151-181. https://doi.org/10.1016/j.quascirev.2017.05.011

Amigo, A., Lara, L.E., Smith, V.C., 2013. Holocene record of large explosive eruptions from Chaitén and Michinmahuida Volcanoes, Chile. Andean Geol. 40, 227-248. https://doi.org/ 10.5027/andgeoV40n2-a03.

Bronk Ramsey, C., Lee, S., 2013. Recent and Planned Developments of the Program OxCal. Radiocarbon 55(2-3), 720-730. https://doi.org/10.2458/azu_js_rc.55.16215.

Bullock, P., Fedoroff, N., Jongerius, A., Stoops, G., Tursina, T., Babel, U., 1985. Handbook for soil thin section description. Waine Res.Publ., Albrighton.

Carn, S.A., Pallister, J.S., Lara, L.E., Ewert, J.W., Watt, S., Prata, A.J., Thomas, R.J., Villarosa, G., 2009. The Unexpected Awakening of Chaitén Volcano, Chile. Eos Trans. AGU 90(24), 205-206.

Castro, J.M., Dingwell, D.B., 2009. Rapid ascent of rhyolitic magma at Chaitén volcano, Chile. Nature 416, 780-783. doi:10.1038/nature08458.

Castro, J.M., Schipper, C.I., Mueller, S., Militzer, A.S., Amigo, A., Parejas, C., Jacob, D., 2013. Storage and eruption of near-liquidus rhyolite magma at Cordón Caulle, Chile. Bull. Volcanol. 75, 1-17. https:/dx./doi.org/10.1007/s00445-013-0702-9.

Cembrano, J., Hervé, F., Lavenu, A., 1996. The Liquiñe Ofqui fault zone: a long living intra-arc fault system in southern Chile. Tectonophysics 259, 55-66. https://doi.org/10.1016/0040-1951(95)00066-6

Dirección Meteorológica de Chile, Departamento de Climatología, 2001. Climatologia regional. Santiago de Chile.

D'Orazio, M., Innocenti, F., Manetti, P., Tamponi, M., Tonarini, S., Gonzales-Ferran, O., Lahsen, A., Omarini, R., 2003. The Quaternary calc-alkaline volcanism of the Patagonian Andes close to the Chile triple junction: Geochemistry and petrogenesis of volcanic rocks from the Cay and Maca volcanoes (~45°S Chile). J.S. Am. Earth Sci. https: /doi.org:10.1016/S0895-9811(03)00063-4.

FAO, 2006. Guidelines for soil description, fourth ed. FAO, Rome.

Garreaud, R.D., 2009. The Andes climate and weather. Adv. Geosci. 22, 3-11. https://doi.org/10.5194/adgeo-22-3-2009, 2009.

Hervé, F., Pankhurst, R.J., Fanning, C.M., Calderón, M., Yaxley, G.M., 2007. The South Patagonian batholith: 150 my of granite magmatism on a plate margin. Lithos 97, 373–394.

Horwell, C.J., Le Blond, J.S., Michnowicz S.A.K., Cressey, G., 2010. Cristobalite in a rhyolitic lava dome: evolution of ash hazard. Bull. Volcanol. 72, 249–253, doi: 10.1007/s00445-009-0327-1.

IUSS Working Group WRB, 2015. World Reference Base for Soil Resources 2014. International soil classification system for naming soils and creating legends for soil maps. World Soil Resour. Rep. No. 106, FAO, Rome. ISBN 978-92-5-108369-7

Kilian, R., López-Escobar, L., 1991. Petrology of the southern South Andean volcanic zone (41–46°S) with emphasis on the Michin máhuida-Chaitén complex (43°S). Zentralbl. Geol. Palaeontol. 6, 1693-1708.

Lara, L.E., Moreno, H., Naranjo, J.A., Matthews, S., de Arce, C.P., 2006. Magmatic evolution of the Puyehue-Cordón Caulle Volcanic Complex (40° S), Southern Andean Volcanic Zone: From shield to unusual rhyolitic fissure volcanism. J Volcanol Geotherm Res 157, 343-366.

Lara, L.E., 2009. The 2008 eruption of the Chaitén Volcano, Chile: a preliminary report. Andean Geol. 36,125-129. ISSN: 0718-7092.

Lara, L.E., Moreno, R., Amigo, A., Hoblitt, R.P., Pierson, T.C., 2013. Late Holocene history of Chaitén Volcano-new evidence for a 17th-century eruption. Andean Geol. 40, 249-261. https://doi.org/10.5027/andgeoV40n2-a04.

López-Escobar, L., Kilian, R., Kempton, P.D., Tagiri, M., 1993. Petrography and geochemistry of Quaternary rocks from the southern volcanic zone between 41° 30' and 46°00' S, Chile. Revista Geologica de Chil e 20, 35-55.

López-Escobar, L., Moreno, R.H., 1994. Geochemical characteristics of the Southern Andes basaltic volcanism associated with the Liquiñe-Ofqui fault zone between 39° and 46°S. Congr. Geol. Chil., No. 7, Ac tas 2, 1388-1393. Concepciòn

Lowenstern, J.B., Sisson, T.W., Pallister, J., Lara, L., Munoz, J., 2008. Explosive eruption of aphyric rhyolitic liquid during May 2008 from Chaitén Volcano, Chile. Eos, Trans American Geophysical Union, Fall Meeting Supplement, Abstract 89(53):V43D-2180.

Lowenstern, J.B., Bleick, H., Vazquez, J.A., Castro, J.M., Larson, P.B., 2012. Degassing of Cl, F, Li, and Be during extrusion and crystallization of the rhyolite dome at Volcán Chaitén, Chile during 2008 and 2009. Bull. Volcanol. 74(10): 2303-2319.

Major, J.J., Lara, L.E., 2013. Overview of Chaitén Volcano, Chile, and its 2008-2009 eruption. Andean Geol. 40,196-215. https://doi.org/10.5027/andgeoV40n2-a01.

Martin, R.S., Watt, S.F.L., Pyle, D.M., Mather, T.A., Matthews, N.E., Georg, R.B., Day, J.A., Fairhead, T., Witt, M.L.I., Quayle, B.M., 2009. Environmental effects of ashfall in Argentina from the 2008 Chaitén volcanic eruption. *J.* Volcanol. Geotherm.184, 462-472. https://doi.org/10.1016/j.jvolgeores.2009.04.010.

McCormac, F.G., Hogg, A.G., Blackwell, P.G., Buck, C.E., Higham, T.F.G., Reimer, P.J., 2004. SHCal04 Southern Hemisphere calibration, 0–11.0 cal kyr BP. Radiocarbon 46(3), 1087–1092.

Mella Barra, M.A., 2008. Petrogêneses do Complexo Vulcânico Yate (42º30'S), Andes do Sul, Chile. PhD Thesis. Univ. Sao Paulo. Doi 10.11606/T.44.2009.tde-e04032009-091537 (http://www.teses.usp.br/teses/disponiveis/44/44141/tde-04032009-091537/fr.php visited on 23/04/2019)

Moreno, P.I., Alloway, B.V., Villarosa, G., Outes, V., Henriquez, W.I., De Pol-Holz, R., Pearce, N.J.G., 2015. A past-millennium maximum in postglacial activity from Volcán Chaitén, southern Chile. Geology 43, 47-50. https://doi.org/10.1130/G36248.1.

Murphy, C.P., 1986. Thin section preparation of soils and sediments. AB Academic Publishers, Berkhamsted, Herts, U.K..

Naranjo, J. A., Stern, C. R., 1998. Holocene explosive activity of Hudson volcano, southern Andes. Bull. Volcanol. 59, 291–306. https://doi.org/10.1007/s004450050193.

Naranjo, J. A., Stern, C.R., 2004. Holocene tephrochronology of the southernmost part (42°30' – 45°S) of the Andean Sou thern Volcanic Zone. Rev. Geol. Chile 31, 224-240.

Nesbitt, H.W., Young, G.M., 1984. Prediction of some weathering trends of plutonic and volcanic rocks based on thermodynamic and kinetic considerations. Geoch. Cosmochim. Acta 48(7), 1523-1534. https://doi.org/10.1016/0016-7037(84)90408-3

Oksanen, J., Guillaume Blanchet, F., Friendly, M., Kindt, R., Legendre, P., McGlinn, D., Minchin, P. R., O'Hara, R.B., Simpson, G. L., Solymos, P., Henry, M., Stevens, H., Szoecs, E., Wagner, H., 2017. vegan: Community Ecology Package. R package version 2.5-3. https://CRAN.R-project.org/package=vegan

Pallister, J.S., Major, J.J., Pierson, T.C., Hoblitt, R.P., Lowenstern, J.B., Eichelberger, J.C., Lara, L.E., Moreno, H., Muñoz, J., Castro, J. M., Iroumé, A., Andreoli, A., Jones, J., Swanson, F., Crisafulli, C., 2010. Interdisciplinary Studies of Eruption at Chaitén Volcano, Chile. Eos Trans. Am. Geophys. Union 91, 381-392.

Pankhurst, R.J., Weaver, S.D., Hervé, F., Larrondo, P., 1999. Mesozoic-Cenozoic evolution of the North Patagonian Batholith in Aysén, southern Chile. J.Geol.Soc. 156, 673-694.

Parada, M.A., Lahsen, A., Palacios, C., 2001. Ages and geochemistry of Mesozoic-Eocene region of the Patagonian Andes (Chile). Rev. Geol. Chile 28, 25-46. https://doi.org/10.4067/S0716-02082001000100002.

Peel, M. C., Finlayson, B. L., McMahon, T. A., 2007. Updated world map of the Köppen-Geiger climate classification. Hydrol. Earth Syst. Sci. 11:1633–1644. https://doi.org/10.5194/hess-11-1633-2007.

Pierson, T.C., Major, J.J., Amigo, A., Moreno, H., 2013. Acute sedimentation response to rainfall following the explosive phase of the 2008-2009 eruption of Chaitén Volcano, Chile. Bull. Volcanol. 75,723. https://doi.org/10.1007/s00445-013-0723-4.

Romero, J.E., 2011. The evolution of the 2008-2011 eruptive cycle at Chaitén volcano, 42°83'S, Southern Chile. Pyroclastic Flow, J.Geol. Vol. 1, nº 1. ISSN 0719-0565. Vol. 1 nº 1.

Schoeneberger, P.J., Wysocky, D.A., Benham, E.C., Soil Survey Staff, 2012. Fieldbook for describing and sampling soils. Version 3.0. Nat. Resour. Cons. Serv., Natl. Soil Surv. Cent., Lincoln, NE.

Sedov, S., Stoops, G., Shoba, S., 2010. Regoliths and soils on volcanic ash, in: Stoops, G., Marcelino, V., Mees, F. (Eds.), Interpretation of Micromorphological Features of Soils and Regoliths. Elsevier, Amsterdam, pp.275-303.

Singer, B.S., Jicha, B.R., Harper, M.R., Naranjo, J.A., Lara, L.E., Moreno-Roa, H., 2008. Eruptive history, geochronology, and magmatic evolution of the Puyehue-Cordón Caulle volcanic complex, Chile. GSA Bulletin 120, 599–618; doi: 10.1130/B26276.1

Stern, C.R., 2008. Holocene tephrochronology record of large explosive eruptions in the southernmost Patagonian Andes. Bull. Volcan. 70 (4), 435-454.

Stern, C.R., García, C., Navarro, X., Muñoz, J., 2009. Fuentes y distribucion de differentes tipos de obsidianas en sitios arqueologicos del centro-sur de Chile (38-44°S). Magallania 37(1), 179-192.

Stoops, G., 2003. Guidelines for the Analysis and Description of Soil and Regolith Thin Sections. SSSA, Madison.

Sun, S.S., McDonough W.F., 1989. Chemical and isotopic systematics of oceanic basalts: implications for mantle composition and processes. Geological Society, London, Special Publications 42, 313-345.

Thiele, R., Hervé, E., Parada, M.A., Godoy, E.,1986. The Liquiñe-Ofqui megafault at the Reloncavi Fiord (41°30' S), Chile. Univ. Chile, Dept. Geol., Comun. 46, 3-15.

Tilling, R. I., 2009. Volcanism and associated hazards: the Andean perspective. Adv. Geosci. 22,125-137.

van Reeuwijk, L.P., 2002. Procedures for Soil Analysis. Technical Paper n. 9. International Soil Reference and Information Centre. Wageningen, Netherlands.

Vásquez, P., Franz, G., 2008. The Triassic Cobquecura Pluton (Central Chile): An example of a fayalite-bearing A-type intrusive massif at a continental margin. Tectonophysics 459, 66–84.

Vásquez, P., Glodny, J., Franz, G., Romer, R.L., Gerdes, A., 2009. Origin of fayalite granitoids: New insights from the Cobquecura Pluton, Chile, and its metapelitic xenoliths. Lithos 110, 181–198.

Watt, S.F.L., Pyle, D.M., Mather, T.A., Martin, R.S., Matthews, N.E., 2009. Fallout and distribution of volcanic ash over Argentina following the May 2008 explosive eruption of Chaitén, Chile. J. Geophys. Res. 114, 1-11. https://doi.org/10.1029/2008JB006219.

Watt, S.F.L., Pyle, D.M., Naranjo, J.A., Rosqvist, G., Mella Barra, M., Mather, T.A., Moreno, H., 2011. Holocene tephrochronology of the Hualaihue region (Andean southern volcanic zone, ~42°S), southern Chile. Quat. Int. 246, 324-343.https://doi.org/10.1016/j.quaint.2011.05.029.

Watt, S.F.L., Pyle, D.M., Mather, T.A., 2013. Evidence of mid- to late-Holocene explosive rhyolitic eruptions from Chaitén volcano, Chile. Andean Geol. 40, 216-226. https://doi.org/10.5027/andgeoV40n2-a02.

Whitney, D.L., Evans, B.W., 2010. Abbreviations for names of rock-forming minerals. Am. Mineral. 95, 185-187.

Wicks, C., de la Llera, J.C., Lara, L.E., Lowenstern, J., 2011. The role of dyking and fault control in the rapid onset of eruption at Chaitén volcano, Chile. Nature 478, 374-377. https://doi.org/10.1038/nature10541.

Zúñiga, F., Dec, D., Valle, S.R., Thiers, O., Paulino, L., Martínez, O., Seguel, O., Casanova, M., Pino, M., Horn, R., Dörner, J., 2019. The waterlogged volcanic ash soils of southern Chile. A review of the "Ñadi" soils. Catena, 173, 99-113.

Table captions

Tab.1: Coordinates of described soil/tephra sections and rock sampling sites

Tab. 2: Morphological and physical properties of soil/tephra sections. *

Tab.3: Chemical characteristics of P16, P17 and P18 sections

Table 4 - Geochemical analyses of studied samples for major elements (wt%), trace and REE (ppm).

Table 5 - Radiocarbon dates for the Chaitén area

Figure captions

Fig. 1. Location map of some volcanoes of the Southern Volcanic Zone (a). The inset (b) shows the location of the investigated field sites in the Chaitén village area and the effects of the 2008 Chaitén eruption.

Fig. 2. Stratigraphic columns of the investigated soil-tephra sequences.

Fig. 3. The studied tephra-layers/soil-horizons sequences before last Chaitén eruption (February 2005): a) P16 section; b) P18 section; c) P17 section.

Fig. 4. Thin section photographs derived from P17-2Btg (a) and P16-3CBd. In P17-2Btg, the red clay mass and the spongy, organic-matter rich coatings on pore walls are well visible; a few black redoximorphic Fe-Mn concentrations are visible as well (frame dimension is 0.5 mm). In P16-3CBd, the compact structureless groundmass is visible, with a few vughs. Fe-Mn nodules and concentrations are visible as well (frame dimension is 5 mm).

Fig. 5. X-Ray diffraction patterns of P18-AE (a) and P18-5CBd (b) samples.

Fig. 6. Representative minerals, lithics and glasses separated from samples P18-AE and P18-5CBd (fraction above 250 µm). Microprobe analyses are shown in supplementary materials (Tab. S1 to S5). P18-AE: a) deep-brown amphibole, Ti-rich tschermakite; unzoned and showing the same features and chemistry as the amphibole found in 2008 Chaitén tephra (Lowenstern et al., 2008; 2012); b) granodiorite lithic; the assemblage (Pl, Kfs, Qz, Hbl, Bt, Ilm, Mag) and mineral chemistry show strong similarities with P18 bed-rock; c) highly vesicular fluidal pumice; d) P18-5CBd: lithic of light-green olivine (Fo_{20}) with glass inclusion and plagioclase; the olivine single crystals are colorless and have higher forsterite content (Fo_{70}).

Fig. 7. Chondrite-normalized REE distribution patterns (a, c, e). Primitive-mantle normalized multi-element (b, d, f) for studied samples. Normalization data are from Sun and McDonough (1989).

Fig. 8. Cluster dendrogram (average linkage clustering method, euclidean distance) of the different samples, based on geochemical composition.

Fig. 9. Refractory inter-element ratio plot. Fields of some volcanoes in the SVZ are compiled from López-Escobar et al. (1993), Mella Barra (2008), Watt et al. (2011), Amigo et al. (2013). Symbols and fields in color are the studied samples.

Table 4 - Geochemical analyses of studied samples for major elements (wt%), trace and REE (ppm).

Site	P16						P17	P18												Chaiten (2008 eruption)			Lago Pinto	Michinmahuida		Corcovado
Sample	Ah	2Bwh2	2Bt	3CBd	4C	5Csm	4CBd	Ah	AE	2Bwh1	2Bwh2	2Bth	3Oa	4Csm	5CBd	6C	7Cs	8C	R-GRD	CHA-1	CHA-2	CHA-3	LP-1	MIC-1	MIC-2	COR-1
Long. (W)	72°42'16"						72°42'53"	72°43'05"												72°42'16"	72°42'52"	72°42'52"	72°19'20"	72°25'44"	72°29'18"	72°51'53"
Lat. (S)	42°54'45"						42°54'39"	42°54'36"												42°54'45"	42°55'03"	42°55'17"	41°51'05"	42°51'14"	42°57'55"	43°14'42"
wt%																										
SiO_2	51.13	28.18	26.81	35.18	43.49	45.32	36.11	46.12	52.61	23.44	22.71	22.37	14.74	21.55	41.25	48.67	43.4	56.78	65.09	74.6	74.37	73.56	70.13	45.95	64.29	52.38
TiO_2	0.62	1.71	2.05	1.83	1.54	1.35	1.80	0.96	0.45	1.48	1.77	1.86	1.22	1.24	1.82	1.51	1.55	1.35	0.55	0.15	0.13	0.14	0.52	1.54	0.98	0.89
Al_2O_3	9.93	22.6	22.97	19.9	19.49	18.88	20.40	11.74	9.48	19.47	21.32	21.54	16.96	14.44	19.2	18.00	19.54	15.7	15.79	14.00	13.79	13.92	13.83	19.66	15.16	18.56
$Fe_2O_3^{tot}$	3.78	12.46	12.93	13.77	10.65	10.21	12.11	3.87	2.12	7.93	4.50	3.73	3.82	32.55	12.06	10.2	10.06	9.85	5.22	1.46	1.4	1.37	3.17	9.52	6.49	8.77
MnO	0.05	0.04	0.06	0.23	0.26	0.25	0.47	0.05	0.04	0.04	0.04	0.04	0.03	0.43	0.22	0.20	0.20	0.15	0.10	0.06	0.06	0.06	0.06	0.16	0.16	0.15
MgO	0.59	1.46	1.87	3.92	2.08	1.15	3.40	0.60	0.43	1.25	1.49	1.47	0.97	1.60	3.4	2.19	1.08	2.03	2.13	0.29	0.27	0.28	0.79	2.97	1.31	5.62
CaO	1.34	1.06	1.55	3.18	3.85	2.09	3.95	1.28	1.51	1.28	1.70	1.71	0.97	1.15	5.01	4.53	2.33	3.67	4.82	1.52	1.36	1.44	2.35	7.66	3.65	9.25
Na_2O	2.30	0.95	0.99	1.22	2.62	2.08	1.62	2.12	2.54	0.85	0.92	0.91	0.52	0.61	2.01	3.12	1.92	2.43	3.34	4.14	4.09	4.17	3.9	3.04	4.88	3.04
K_2O	1.59	0.48	0.39	0.45	0.87	0.98	0.42	1.41	1.75	0.36	0.28	0.26	0.18	0.22	0.52	1.07	0.79	1.07	2.4	3.02	3.13	3.07	3.42	0.84	2.55	0.65
P_2O_5	0.13	0.14	0.2	0.40	0.49	0.20	0.59	0.13	0.11	0.17	0.21	0.23	0.17	0.18	0.62	0.46	0.22	0.08	0.1	0.06	0.05	0.05	0.12	0.41	0.33	0.15
LOI	28.4	30.7	30.0	19.6	14.4	17.2	18.9	31.6	28.8	43.6	44.9	45.7	60.3	25.8	13.6	9.8	18.7	6.7	0.3	0.6	1.2	1.8	1.5	8.0	0	0.3
Sum	99.98	99.89	99.88	99.86	99.89	99.89	99.84	99.95	99.98	99.93	99.92	99.92	99.94	99.85	99.86	99.89	99.91	99.81	99.85	100.01	99.98	99.96	99.94	99.89	99.97	99.85
TOT/C	11.65	3.86	3.55	0.83	0.34	0.79	0.95	11.71	14.19	10.09	11.07	11.52	19.62	2.21	0.30	0.08	1.14	0.39	0.00	0.12	0.06	0.04	0.1	1.33	0.04	0.08
CIA	55.56	84.93	82.50	70.62	61.39	69.50	66.44	61.52	51.80	82.55	81.28	81.50	85.77	81.24	59.66	55.33	70.31	57.25	48.36	52.15	52.27	52.08	49.00	49.77	46.52	45.17
ppm																										
Cr	27	55	62	62	27	75	48	34	bdl	48	41	41	34	34	48	14	103	bdl	bdl	bdl	bdl	bdl	bdl	bdl	bdl	68
Sc	6	38	41	38	34	26	37	10	5	31	36	34	27	28	35	31	26	20	13	3	2	9	2	27	19	27
Mo	0.5	1.1	1.1	0.6	1.4	1.2	1.8	0.5	0.3	0.9	0.6	0.5	0.5	1.1	0.7	0.8	1.1	1.2	0.5	0.2	0.3	0.3	0.3	0.3	0.8	0.1
Cu	6.4	54.9	44.4	72.7	42.1	21.1	52.7	7.3	4.1	29.7	39.6	43.1	25.5	50.7	59.4	36.5	21.1	21.3	9.9	0.3	2.7	4.2	3.5	92.9	10.8	23.4
Pb	9.3	17.4	16.2	13.5	18.3	17	11.2	9.6	7	11.7	12.8	12.6	12	9.5	11.7	15.4	17.6	12.5	1.5	1.7	3.3	4	5.4	7.7	53.4	1.8
Zn	7	59	65	94	78	62	68	9	12	40	52	58	45	76	73	74	52	35	31	4	6	16	2	58	46	23
Ni	2.5	18.5	19.1	27.9	12.1	8.8	18.1	2.1	1.3	9.8	14.6	16.4	10.1	22.4	21.4	8.2	5	6.7	bdl	0.4	5.1	7	5.2	13.6	2.6	22.5
As	5.4	6.5	4.2	4.8	5.8	5.3	4.7	3.6	1.5	5.3	3.3	3.3	4.1	5	5.1	5.1	4.6	2.2	0.8	1.3	2.4	0.9	0.9	1.3	1	bdl
Au (*ppb*)	6	3.8	2.9	19	25.4	7.6	0.9	21.9	2	bdl	1.7	0.7	bdl	1.9	1.2	2.2	6.3	bdl	1.9	bdl	bdl	1.7	bdl	bdl	0.7	bdl
Ba	373	206	211	516	359	719	306	368	453	148	176	200	186	218	356	465	590	482	435	659	656	658	669	335	597	199
Be	1	bdl	bdl	2	2	3	2	1	2	1	2	2	1	2	1	3	3	bdl	bdl	2	2	2	3	3	3	bdl
Co	2.3	14.2	16.3	36.2	20.3	19.1	46.7	3.6	2.4	9.0	11.8	11.6	10.4	58.3	26.9	17.2	11.4	13.6	11.0	1.0	0.8	6.6	0.9	21.2	5.7	30.4
Cs	4.0	1.4	1.2	1.7	1.8	2.4	1.7	3.7	4.9	0.9	0.9	1.0	0.9	1.1	1.4	2.1	1.8	1.6	2.8	7.2	7.1	4.3	7.4	1.6	3.3	0.8
Ga	14.0	22.1	24.3	20.8	21.7	24.5	21.9	17.7	12.2	20.9	22.8	23.2	21.7	16.3	19.9	23.0	28.1	25.1	14.7	13.2	12.9	15.7	12.5	19.2	18.2	16.4
Hf	3	6	6.9	5.5	8.9	8.6	5.7	4.1	3.2	5.5	6	6.1	5.8	4.5	5.9	10.9	8.7	3.8	4.1	3.7	3.3	6.6	3.6	4.9	9.7	2.2
Nb	8.3	11	13.4	10.4	17.1	16	10.6	10.5	8.1	9.7	10.5	11.1	11.5	7.7	10.2	19.3	16.2	9.9	4.8	8.6	8.6	6.4	17.9	9.2	16.7	2.8
Rb	58	17	11	13	23	32	12	59	73	12	8	7	10	6	15	31	25	27	74	110	110	94	109	23	68	15
Sr	113	88	114	181	256	177	221	129	145	99	126	141	181	88	287	288	231	207	254	150	142	258	147	439	285	389
Ta	0.6	0.9	1	0.6	1	1.1	0.7	0.8	0.6	0.6	0.6	0.6	0.6	0.5	0.6	0.9	1.1	0.6	0.4	0.9	0.9	0.5	4.4	0.6	1.1	0.2
Th	8.1	6.3	6	4.7	8.7	11.2	4.3	9.5	8.9	6.0	4.9	5.1	5.1	3.6	4.5	9.1	9.1	6.8	7.3	12.6	13.5	10.6	12.8	3.8	8.4	2.1
U	2.6	1.8	1.6	1.2	2.1	3.2	1.5	2.7	2.6	1.7	1.4	1.4	1.1	0.9	1.4	2.2	3.2	2.1	1.2	3.5	3.7	2.6	3.7	1.2	2.5	0.5
V	72	276	346	276	178	223	286	114	49	276	261	214	269	268	258	181	234	239	106	bdl	bdl	86	bdl	222	29	217
W	3.0	1.5	1.0	0.7	1.5	2.8	0.8	3.1	3.1	1.1	0.8	0.8	0.9	0.6	1.0	1.7	2.0	1.8	bdl	4.7	4.6	1.7	4.2	bdl	1.5	bdl
Zr	102	226	242	213	361	306	208	140	98	205	209	220	222	170	212	405	304	153	134	105	99	220	110	182	366	82
Y	11.3	20.4	28.5	28.5	43.6	53.8	39.8	12.3	10.9	25.0	31.9	30.4	25.0	27.9	44.8	64.4	65.9	60.7	20.1	11.9	12.1	26.0	11.3	36.9	52.4	17.3
La	16.6	10.6	10.8	17.8	24.6	32.6	22.6	16.2	17.2	13.9	19.0	18.7	14.3	18.8	23.6	35.9	35.8	42.3	18.4	23.9	24.0	23.5	21.7	19.7	32.0	8.8
Ce	33	37.9	44.8	64.8	101.8	132.7	101.6	34.7	33.8	44.3	57.0	52.7	40.8	66.5	71.1	96.9	78.7	46.6	37.0	47.5	47.5	47.5	48.9	50.3	77.6	21.4
Pr	3.55	5.14	6.33	6.4	8.68	11.27	7.27	3.76	3.71	5.42	6.54	6.32	4.88	5.46	7.95	11.33	10.56	10.28	4.18	4.88	4.94	4.89	5.82	6.52	9.83	2.76
Nd	13.1	24.4	28.8	28.5	38.4	49.6	32.0	15.0	12.7	24.1	29.1	29.3	21.9	23.9	34.7	48.7	45.0	41.1	16.7	17.6	17.0	17.6	24.1	30.3	43.4	13.4

Sm	2.08	5.72	7.36	5.97	8.48	10.56	7.12	2.49	2.11	5.5	6.59	6.06	4.91	5.00	7.4	10.45	8.84	9.23	3.41	2.55	2.56	2.61	4.61	6.44	8.81	2.91
Eu	0.49	1.54	2.08	1.70	2.25	2.47	1.9	0.68	0.5	1.52	1.84	1.75	1.46	1.39	1.98	2.49	2.09	2.12	0.91	0.5	0.47	0.48	0.98	1.76	2.02	0.95
Gd	1.95	5.35	7.28	5.92	8.3	10.63	7.13	2.36	1.8	5.43	6.59	6.3	5.1	5.07	7.9	10.51	9.81	10.49	3.35	2.05	1.92	1.88	4.35	6.77	8.64	3.06
Tb	0.32	0.89	1.21	0.99	1.39	1.73	1.22	0.41	0.31	0.95	1.12	1.08	0.87	0.87	1.28	1.78	1.63	1.54	0.53	0.33	0.34	0.32	0.73	1.1	1.48	0.53
Dy	1.87	5.34	7.16	5.84	8.49	10.34	7.22	2.27	1.68	5.17	6.67	6.01	5.18	4.83	7.49	10.48	9.44	8.68	3.38	1.87	1.86	1.87	4.31	6.23	8.87	3.21
Ho	0.36	1.05	1.47	1.18	1.7	2.09	1.47	0.43	0.33	1.04	1.33	1.22	1.02	1.01	1.57	2.19	2.01	2.00	0.75	0.38	0.38	0.36	0.93	1.35	1.83	0.65
Er	1.04	3.08	4.38	3.32	5.00	6.34	4.31	1.25	1.08	2.97	3.65	3.36	2.8	2.99	4.45	6.74	6.00	6.03	2.16	1.15	1.2	1.16	2.85	3.76	5.43	1.92
Tm	0.17	0.50	0.66	0.52	0.76	0.97	0.65	0.2	0.17	0.44	0.56	0.48	0.42	0.43	0.63	0.99	0.87	0.85	0.32	0.18	0.17	0.2	0.43	0.56	0.84	0.29
Yb	1.19	3.35	4.52	3.52	5.32	6.66	4.26	1.44	1.17	2.88	3.52	3.17	2.78	2.88	4.26	6.49	5.52	4.77	2.24	1.28	1.32	1.29	2.84	3.66	5.48	1.94
Lu	0.18	0.51	0.69	0.51	0.78	1.00	0.64	0.21	0.19	0.42	0.51	0.45	0.41	0.42	0.64	1.01	0.88	0.83	0.36	0.21	0.21	0.21	0.46	0.55	0.86	0.29

bdl - below detection limits

Table 5 - Radiocarbon dates for the Chitén area

Site No.	Location	Sample No.	Radiocarbon age, years BP (±1σ)	*Calibrated age range, cal. years BP
P16	W72°42'16"/S42°54'45"	P16-5Csm	8230±60	9397-8998
P17	W72°42'53"/S42°54'39"	P17-4CBd	7670±60	8558-8317
P18	W72°43'05"/S42°54'36"	P18-Ah	345±30	454-304
		P18-AE	1320±30	1283-1087
		P18-7Cs	9110±60	10407-9935

*Calibrated using OxCal4.2 (Bronk Ramsey and Lee, 2013) and the Southern Hemisphere calibration curve SHCal04 (McCormac et al., 2004), BP refers to years before 1950 A.D.

Tab.1: Coordinates of described soil/tephra sections and rock sampling sites

Sample	Long. [° W]	Lat. [° S]	Sample type & Location	Elevation [m asl]
P16	72°42'16"	42°54'45"	soil section – north Chaitén village	25
P17	72°42'53"	42°54'39"	soil section – La Tranquera	49
P18	72°43'05"	42°54'36"	soil section – Piedra Blanca	22
CHA-1	72°42'16"	42°54'45"	ash - Piedra Blanca	25
CHA-2	72°42'52"	42°55'03"	pumice - Puente Los Gigios	2
CHA-3	72°42'52"	42°55'17"	coarse pumice - south Chaitén village	5
LP-1	72°19'20"	41°51'05"	rhyolite - Lago Pinto Concha	915
MIC-1	72°25'44"	42°51'14"	dacite - Michinmahuida	1300
MIC-2	72°29'18"	42°57'55"	stream sediment - Michinmahuida	271
COR-1	72°51'53"	43°14'42"	basalt - Corcovado	42

Tab. 2: Morphological and physical properties of soil/tephra sections. *

Profile	Horizon or layer	Depth (cm)	Munsell colour (dry)	Horizon boundary	Field description	Structure	Consistence (moist)	Cementation
P16	**0i**	5-0	black (10YR 2/1)	abrupt and smooth	litter of fresh vegetal fibres	laminar	friable	not cemented nor compacted
	Ah	0-30	very dark brown (10YR 2/2)	clear and smooth	organic matter-rich modern horizon	weak and granular	friable	not cemented nor compacted
	2Bwh1	30-50	dark brown (10YR 3/3)	clear and smooth	buried weathered horizon	blocky and subangular	friable	not cemented nor compacted
	2Bwh2	50-75	brown (10YR 4/3)	abrupt and smooth	buried weathered horizon with lapilli ghosts	blocky and subangular	friable	not cemented nor compacted
	2Bt	75-125	dark yellowish brown (10YR 4/4)	abrupt and wavy	buried illuvial horizon with clay coatings and lapilli ghosts	blocky and subangular	friable	not cemented nor compacted
	3CBd	125-245	very dark greyish brown (10YR 3/2) and light brown (7.5YR 6/4)	abrupt and wavy	moderately weathered dense cineritic layer with phytorelicts(hardpan)	blocky and angular	hard	continuos compacted but not cemented
	4C	245-265	brown (7,5YR 4/4)	abrupt and smooth	weathered reddish and black lapilli low to moderate resistant to excavation	massive	very hard	broken compacted but not cemented
	5Csm	265-270	brown (10YR 4/3)	abrupt and smooth	ferruginous pan of weathered lapilli	massive	slightly hard	moderately cemented
	6C	270-275	grey (10YR 5/1)	abrupt and wavy	weathered grey ash	single grain	loose	not cemented nor compacted
	R	275-350+	-	-	greyish metapelites - bedrock	-	-	-
P17	**0i**	3-0	black (10YR 2/1)	abrupt and smooth	litter of fresh vegetal fibres	laminar	friable	not cemented nor compacted
	Ah	0-35	very dark brown (10YR 2/2)	clear and smooth	organic matter-rich, high porous modern horizon	moderate blocky subangular	friable	not cemented nor compacted
	2Bwh1	35-52/53	yellowish brown (10YR 5/3)	gradual and smooth	buried with infilled burrows, weathered horizon	blocky subangular/granular	friable	not cemented nor compacted
	2Bwh2	52/53-80	brown (10YR 5/4)	clear and smooth	buried weathered horizon with fine concentration of organic matter	blocky and subangular	friable	not cemented nor compacted
	2Bth1	80-110	brown (10YR 4/3)	clear and smooth	buried illuvial horizon with few small lithics	moderate to strong coarse prismatic	slightly hard	not cemented nor compacted
	2Bth2	110-150	dark grayish brown (10YR4/2)	clear and smooth	buried illuvial horizon with few rusty mottles and common lithic ghosts	moderate to strong blocky subangular	firm	not cemented, moderately compacted
	2Bth3	150-230	dark brown (10YR3/3)	abrupt and smooth	buried illuvial horizon with many fine lithics	moderate to strong coarse prismatic	firm	compacted but not cemented,
	2Btgd	230-340	dark brown (10YR3/3) with many rusty mottles	abrupt and irregular	buried illuvial gleyed horizon with common lapilli ghosts	moderate to strong coarse prismatic	firm	compacted but not cemented,
	3CBd	340-380+	very dark grayish brown (10YR3/2)	unknown	hardpan - moderately weathered dense cineritic layer with phytorelicts and common lapilli	massive	hard	continous compacted but not cemented

(Table 2 continued)

Profile	Horizon or layer	Depth (cm)	Munsell colour (dry)	Horizon boundary	Field description	Structure	Consistence (moist)	Cementation
P18	**0i**	2/5-0	black (10YR 2/1)	abrupt and smooth	litter of fresh vegetal fibres	laminar	friable	not cemented nor compacted
	Ah	0-9	very dark brown (10YR 2/2)	clear and smooth	organic matter-rich modern horizon	weak and granular	friable	not cemented nor compacted
	AE	9-30	very dark greyish brown (10YR 3/2)	clear and wavy	very rich in organic matter modern horizon	weak and granular	friable	not cemented nor compacted
	2Bwh1	30-100	dark brown (10YR 3/3)	clear and smooth	buried organic matter-rich weathered horizon	blocky and subangular	friable	not cemented nor compacted
	2Bwh2	100-135	brown (10YR 4/3)	clear and wavy	buried organic matter-rich weathered horizon	blocky and subangular	friable	not cemented nor compacted
	2Bth	135-180	dark yellowish brown (10YR 4/4)	abrupt and wavy	buried organic matter-rich illuvial horizon with some argillans	blocky and subangular	friable	not cemented nor compacted
	3Oa	180-182	very dark greyish brown (10YR 3/2) and light brown (7.5YR 6/4)	abrupt and wavy	buried organic horizon	laminar	friable	not cemented nor compacted
	4Csm	182-185	brown (7,5YR 4/4)	abrupt and smooth	Fe cemented ash layer	massive	very hard	continuos cemented
	5CBd	185-292	brown (10YR 4/3)	abrupt and smooth	moderately weathered dense cineritic layer hardpan	massive	hard	compacted but not cemented
	6Cr	292-306	grey (10YR 5/1) and strong brown (7.5YR 5/6)	abrupt and wavy	weathered grey lapilli low to moderate resistant to excavation	single grain	loose	not cemented nor compacted
	7Cs	306-325	dark reddish brown (5YR 3/3)	clear and wavy	reddish ferruginous ash	massive	slightly hard	continous weakly cemented
	8C	325-345	dark yellowish brown (10YR 4/4)	abrupt and irregular	granodiorite alterite mixed with weakly weathered (grey) volcanic ash with some rock fragments	single grain	friable	not cemented nor compacted
	R	345-400+	-	-	sheep-back shaped granodiorite - bedrock	-	-	continuos hard rock

* Descriptions according to FAO (2006) and Schoeneberger et al. (2012)

Tab.3: Chemical characteristics of P16, P17 and P18 sections

Section	Horizon – layer	Depth	pH (H_2O)	pH (NaF)	Organic Matter	CEC	Exch. bases Ca^{++}	Exch. bases Mg^{++}	Exch. bases Na^{+}	Exch. bases K^{+}	Base sat	Al_t total	Al_o oxalate	Fe_t total	Fe_d dithionite	Fe_o oxalate	Fe_o/Fe_d	Fe_d/Fe_t	Fe_o/Fe_t	$(Fe_d-Fe_o)/Fe_t$
		(cm)			($g{*}kg^{-1}$)	($cmol{*}kg^{-1}$)					(%)	($g{*}kg^{-1}$)								%
P16	Ah	0-30	4.2	9.6	141	36.90	1.10	0.58	0.23	0.17	6	6.4	7.0	26.4	13.5	11.9	0.88	0.61	0.45	6.3
	2Bwh2	50-75	5.5	11.0	35	18.30	0.56	0.26	0.12	0.03	5	38.1	19.3	87.1	31.6	3.1	0.10	0.41	0.04	32.6
	2Bt	75-125	5.6	11.1	33	18.60	0.37	0.13	0.06	0.03	3	37.8	19.6	90.4	34.7	3.8	0.11	0.44	0.04	34.1
	3CBd	125-245	5.6	11.0	8	23.80	0.90	0.23	0.21	0.08	6	28.1	18.4	96.3	22.3	7.7	0.35	0.26	0.08	15.1
	4C	245-265	5.7	10.6	3	18.70	0.80	0.22	0.10	0.06	6	28.9	13.9	74.5	13.1	7.8	0.59	0.16	0.10	7.1
	5Csm	265-270	5.6	10.6	7	25.40	1.30	0.47	0.27	0.20	9	49.5	14.1	71.4	32.8	13.3	0.41	0.45	0.19	27.3
P17	Ah	0-35	5.3	11.6	77	38.30	0.51	0.17	0.10	0.07	2	35.3	18.5	53.6	20.7	18.1	0.82	0.39	0.34	4.8
	2Bwh1	35-52/53	5.3	11.4	61	33.50	0.62	0.27	0.04	0.02	3	32.6	18.5	57.1	23.7	13.7	0.58	0.41	0.24	17.6
	2Bwh2	52/53-80	5.5	11.4	49	29.00	0.83	0.28	0.06	0.02	4	32.9	18.9	58.6	24.5	10.9	0.45	0.43	0.19	23.2
	2Bth1	80-110	5.6	11.1	37	24.20	0.58	0.21	0.05	0.02	3	38.6	20.2	62.9	26.3	7.2	0.27	0.42	0.11	30.5
	2Bth2	110-150	5.8	11.0	31	23.10	0.82	0.55	0.09	0.02	6	34.9	18.7	70.6	25.4	6.2	0.24	0.36	0.09	27.3
	2Bth3	150-230	5.8	11.0	27	22.60	0.47	0.16	0.21	0.05	4	49.0	18.5	68.2	27.1	5.3	0.20	0.37	0.08	31.9
	2Btgd	230-340	5.8	11.0	32	23.00	0.48	0.17	0.11	0.03	3	45.7	19.1	93.0	39.9	5.1	0.13	0.45	0.05	37.4
	3CBd	340-380	5.7	10.8	10	26.30	1.22	0.23	0.11	0.07	6	32.3	17.2	84.7	18.7	6.0	0.32	0.22	0.07	15.0
P18	Ah	0-9	4.4	10.8	99	27.80	0.75	0.25	0.17	0.10	5	36.9	11.5	27.1	8.9	7.8	1.00	0.28	0.29	4.1
	AE	9-30	3.7	7.1	140	34.10	4.15	1.05	0.30	0.30	17	21.9	2.0	14.8	2.2	1.6	0.97	0.11	0.11	4.0
	2Bwh1	30-100	4.8	11.5	97	29.10	0.29	0.12	0.07	0.03	2	43.5	17.7	55.5	17.3	12.7	0.73	0.32	0.23	8.4
	2Bwh2	100-135	4.9	11.6	100	43.00	4.51	0.34	0.10	0.02	12	42.0	17.9	31.5	7.4	5.1	0.70	0.20	0.16	7.1
	2Bth	135-180	4.9	11.6	112	54.30	0.59	0.16	0.09	0.01	2	44.9	17.6	26.1	4.1	1.8	0.44	0.12	0.07	8.8
	3Oa	180-182	5.4	11.7	196	68.10	2.40	0.33	0.20	0.06	4	33.3	18.3	26.7	7.3	6.2	0.85	0.23	0.23	4.1
	4Csm	182-185	5.5	10.7	21	33.70	1.22	0.28	0.14	0.08	5	28.5	12.6	227.7	142.9	32.4	0.23	0.61	0.14	48.5
	5CBd	185-292	5.6	10.3	2	15.50	1.63	0.30	0.19	0.10	14	35.7	10.0	84.4	14.0	10.8	0.77	0.17	0.13	3.9
	6C	292-306	5.9	9.7	1	10.20	1.95	0.43	0.17	0.18	27	19.7	8.0	71.3	11.4	5.7	0.50	0.16	0.08	7.9
	7Cs	306-325	5.8	10.2	10	29.50	4.57	0.89	0.48	0.58	22	49.6	13.0	70.4	30.3	12.3	0.41	0.44	0.17	25.6

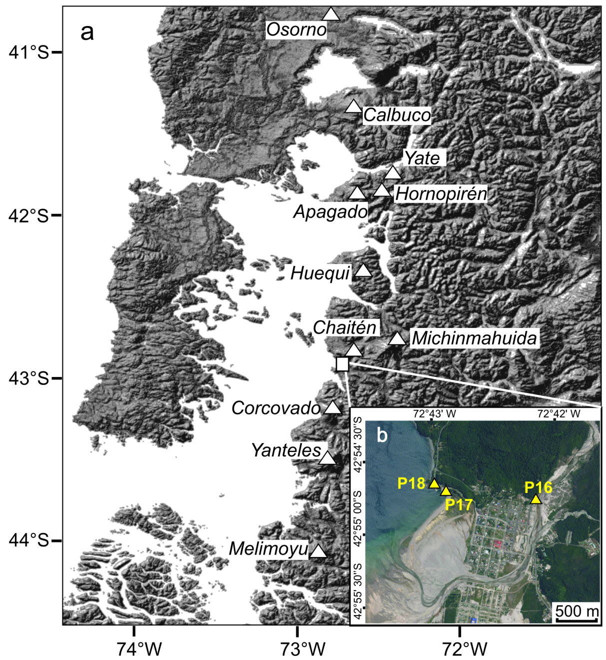
a
Osorno
Calbuco
Yate
Hornopirén
Apagado
Huequi
Chaitén
Michinmahuida
Corcovado
Yanteles
Melimoyu
41°S
42°S
43°S
44°S
74°W
73°W
72°W
b
72°43' W
72°42' W
42°54' 30"S
42°55' 00"S
42°55' 30"S
P18
P17
P16
500 m

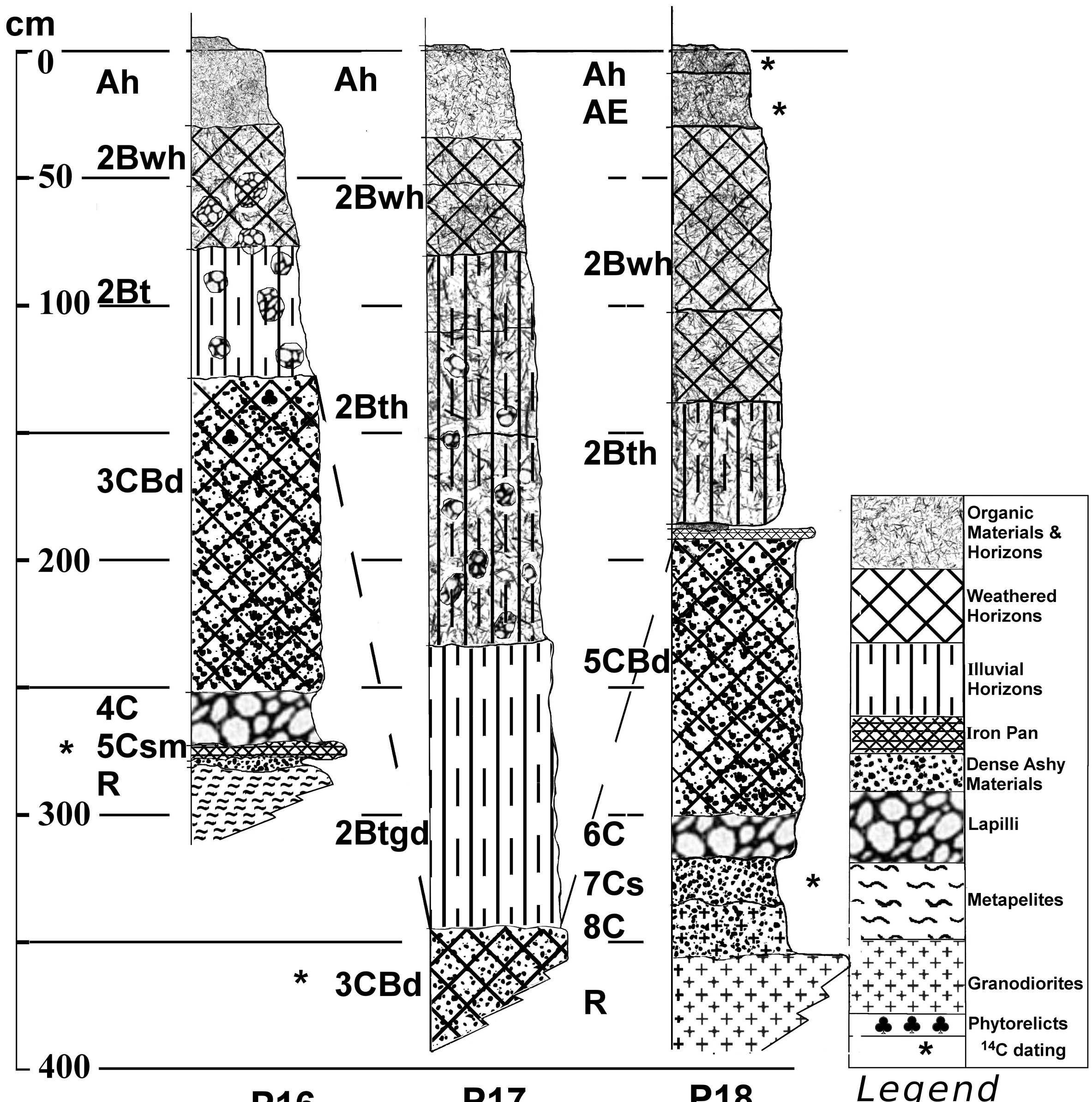

cm
0
50
100
200
300
400
Ah
2Bwh
2Bt
3CBd
4C
*
5Csm
R
Ah
2Bwh
2Bth
2Btgd
*
3CBd
Ah
*
AE
*
2Bwh
2Bth
5CBd
6C
7Cs
*
8C
R
P16
P17
P18
Organic Materials & Horizons
Weathered Horizons
Illuvial Horizons
Iron Pan
Dense Ashy Materials
Lapilli
Metapelites
Granodiorites
Phytorelicts
*
14C dating
Legend

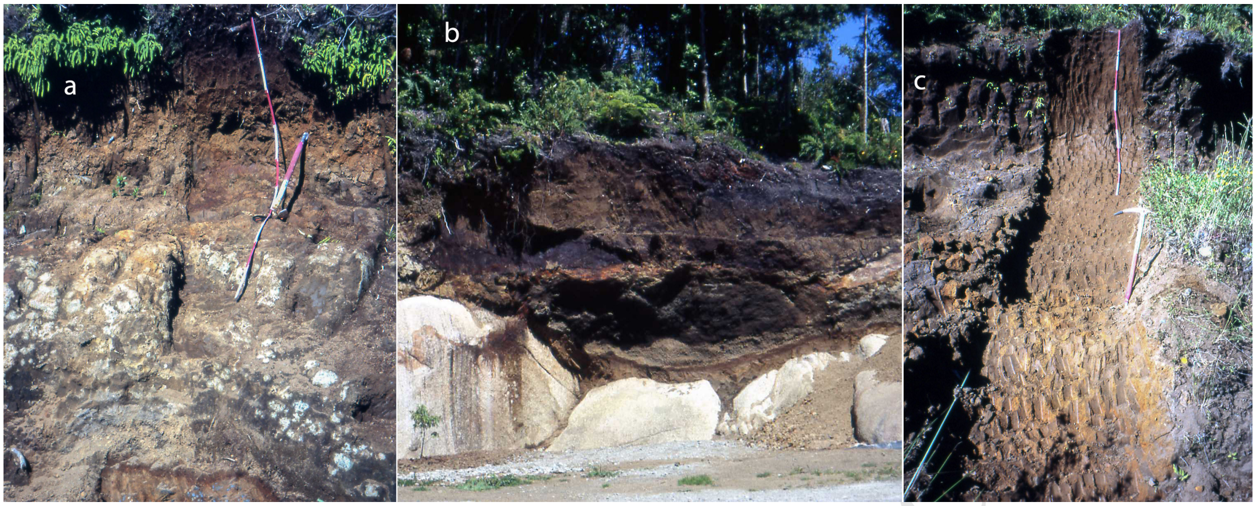
a
b
c

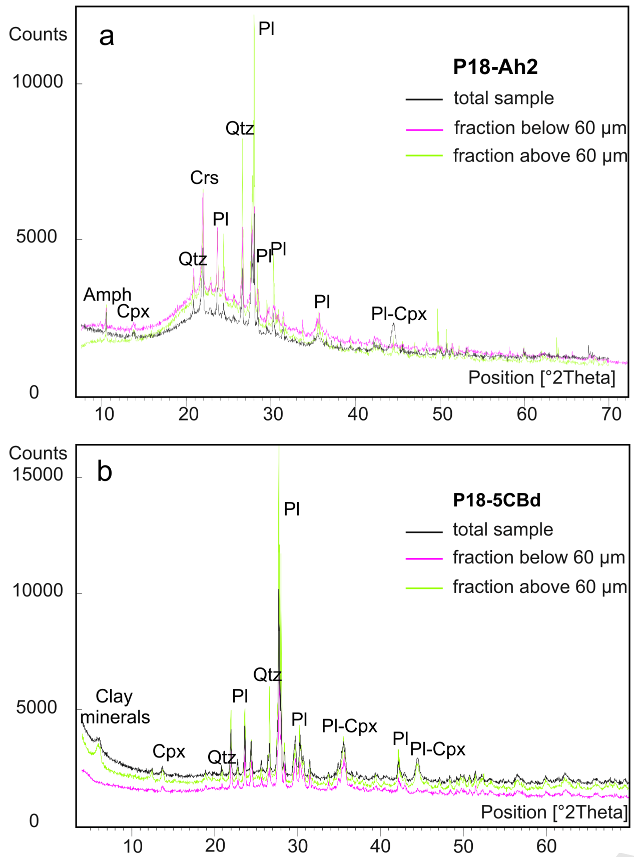
Counts
a
P18-Ah2
total sample
fraction below 60 µm
fraction above 60 µm
10000
5000
0
Pl
Qtz
Crs
Pl
Qtz
Pl
Pl
Amph
Cpx
Pl
Pl-Cpx
Position [°2Theta]
10 20 30 40 50 60 70
Counts
15000
b
P18-5CBd
total sample
fraction below 60 µm
fraction above 60 µm
10000
5000
0
Pl
Clay
minerals
Cpx
Qtz
Pl
Qtz
Pl
Pl-Cpx
Pl
Pl-Cpx
Position [°2Theta]
10 20 30 40 50 60

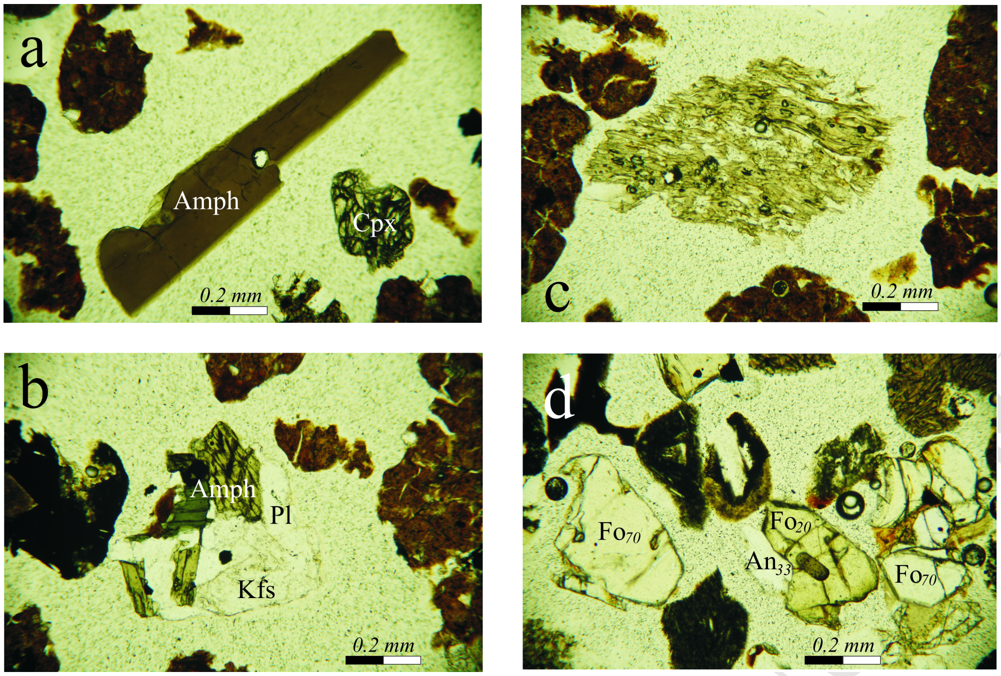
a
Amph
Cpx
0.2 mm
c
0.2 mm
b
Amph
Pl
Kfs
0.2 mm
d
Fo70
Fo20
An33
Fo70
0.2 mm

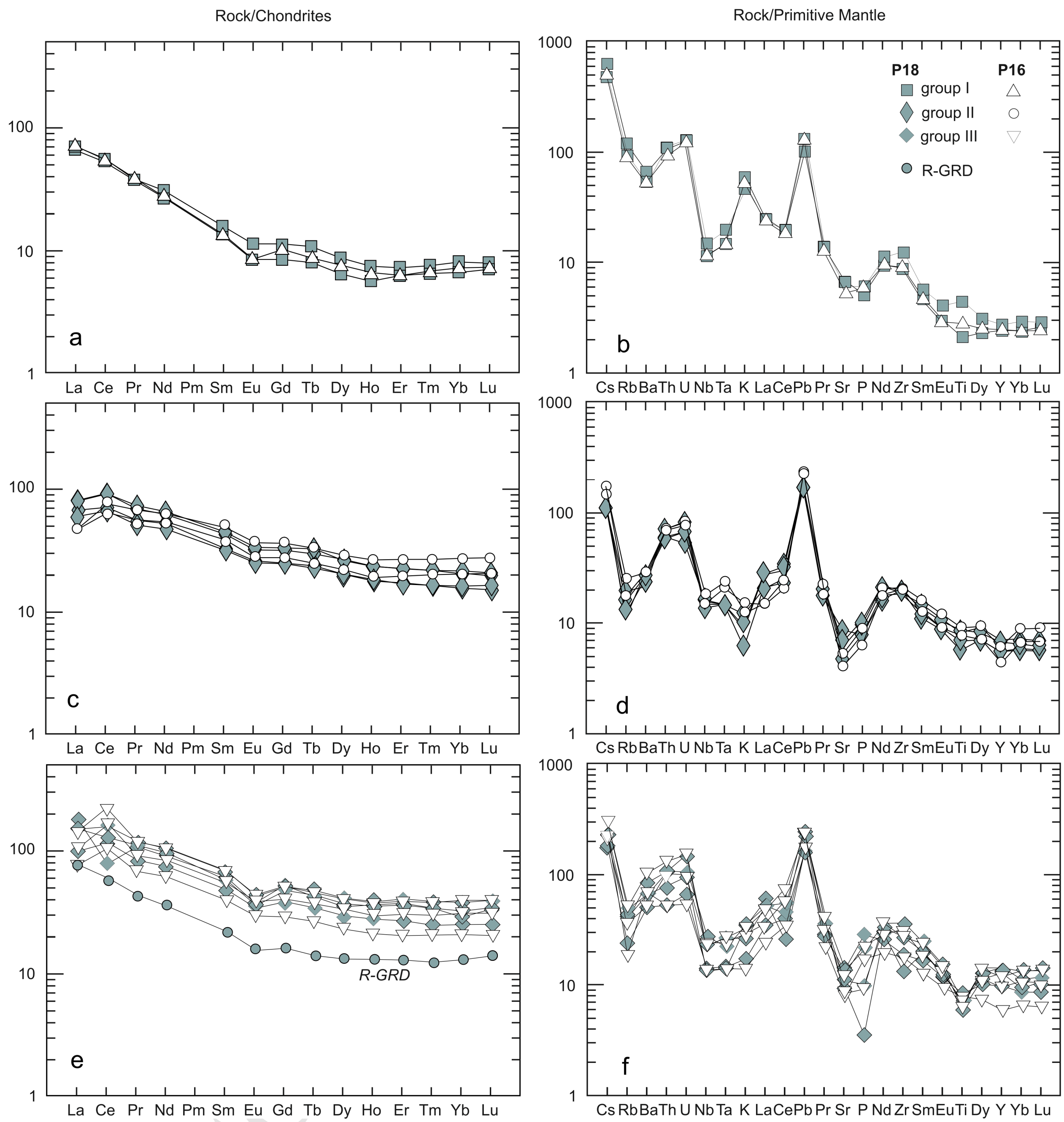
Rock/Chondrites
Rock/Primitive Mantle
P18
P16
group I
group II
group III
R-GRD
1000
100
10
1
La Ce Pr Nd Pm Sm Eu Gd Tb Dy Ho Er Tm Yb Lu
Cs Rb Ba Th U Nb Ta K La Ce Pb Pr Sr P Nd Zr Sm Eu Ti Dy Y Yb Lu
a
b
c
d
e
f
R-GRD

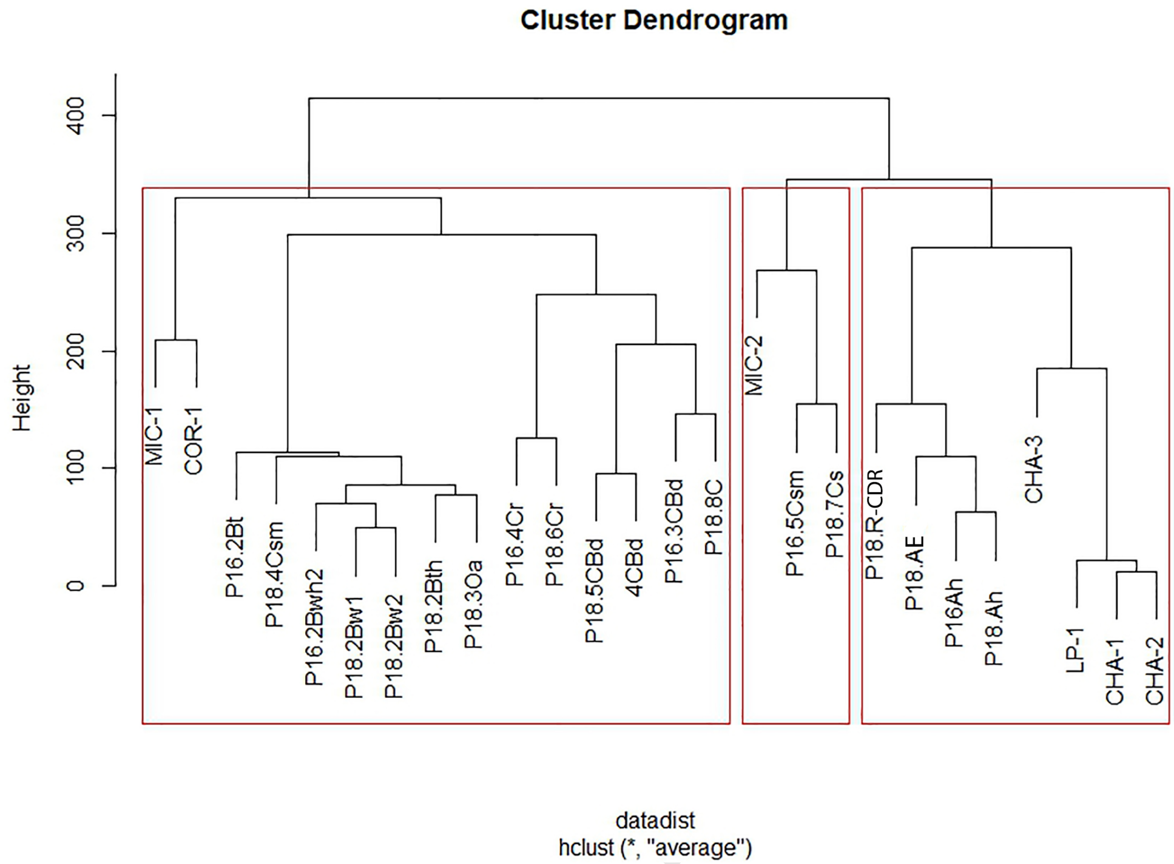

Cluster Dendrogram
Height
0
100
200
300
400
MIC-1
COR-1
P16.2Bt
P18.4Csm
P16.2Bwh2
P18.2Bw1
P18.2Bw2
P18.2Bth
P18.3Oa
P16.4Cr
P18.6Cr
P18.5CBd
4CBd
P16.3CBd
P18.8C
MIC-2
P16.5Csm
P18.7Cs
P18.R-CDR
P18.AE
P16Ah
P18.Ah
CHA-3
LP-1
CHA-1
CHA-2
datadist
hclust (*, "average")

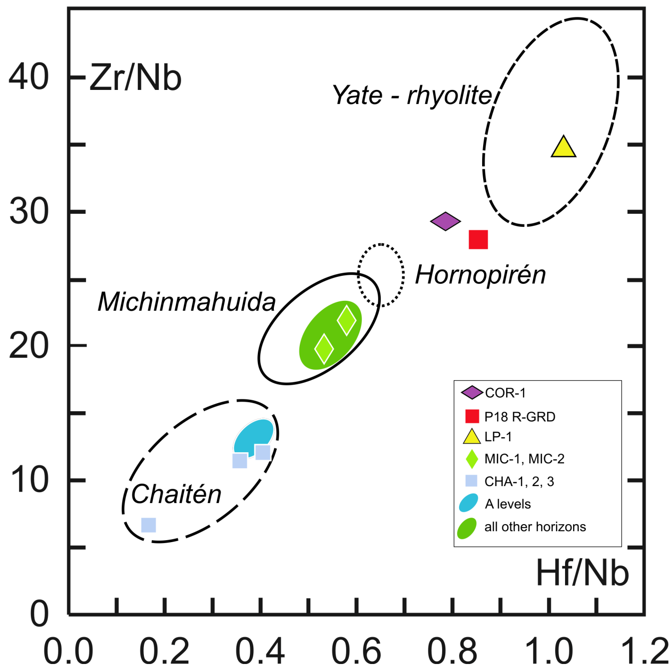

Zr/Nb
40
30
20
10
0
Yate - rhyolite
Hornopirén
Michinmahuida
Chaitén
COR-1
P18 R-GRD
LP-1
MIC-1, MIC-2
CHA-1, 2, 3
A levels
all other horizons
Hf/Nb
0.0
0.2
0.4
0.6
0.8
1.0
1.2

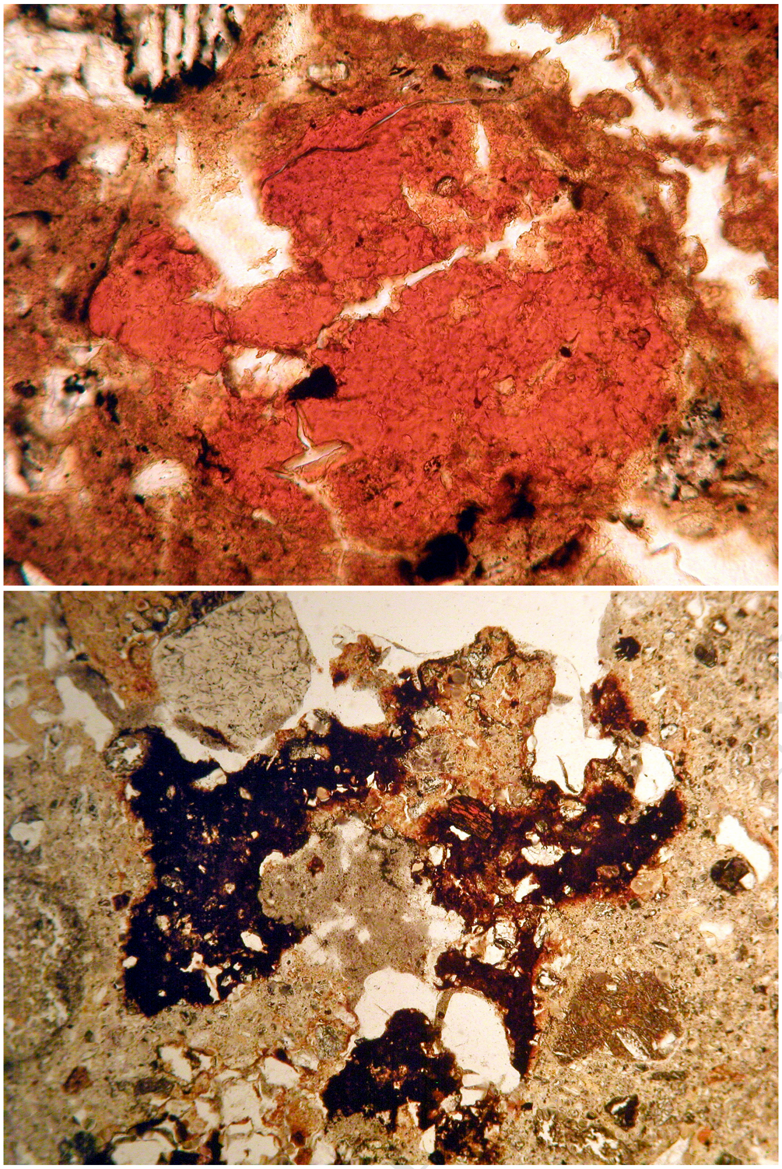

Highlights

- Modern soils, paleosols and tephra have been studied in a volcanic area in Chilean Patagonia
- The integrated approach of pedology, micromorphology, geochemistry and mineralogy has allowed to reconstruct the evolution of soils and to recognize their genesis from pyroclastic materials coming from two different eruptive centers
- The validity of the evolutionary model was ascertained by comparing the dates measured by ^{14}C in the different soils studied, with the chronology of volcanic events recognized by recent geological studies in the area